

# Next-to-Leading Order Corrections to Single Top Quark Production and Decay at the Tevatron: 2. $t$ -channel Process

Qing-Hong Cao,<sup>\*</sup> Reinhard Schwienhorst,<sup>†</sup> Jorge

A. Benitez,<sup>‡</sup> Raymond Brock,<sup>§</sup> and C.-P. Yuan<sup>¶</sup>

*Department of Physics & Astronomy,*

*Michigan State University, East Lansing, MI 48824, USA*

## Abstract

We present a study of the  $t$ -channel mode of single top quark production at the upgraded Tevatron  $p\bar{p}$  collider, including the next-to-leading order (NLO) QCD corrections to the production and the decay of a single top quark. The narrow width approximation was adopted in order to preserve the spin of the top quark in its production and decay. We discuss the effects of different  $O(\alpha_s)$  contributions on the inclusive cross section as well as various kinematic distributions after imposing the relevant cuts to select  $t$ -channel single top signal events.

PACS numbers: 12.38.Bx;13.85.-t;13.88.+e;14.65.Ha

---

<sup>\*</sup>Electronic address: cao@pa.msu.edu

<sup>†</sup>Electronic address: schwer@pa.msu.edu

<sup>‡</sup>Electronic address: benitez@pa.msu.edu

<sup>§</sup>Electronic address: brock@pa.msu.edu

<sup>¶</sup>Electronic address: yuan@pa.msu.edu

## I. INTRODUCTION

In the Standard Model (SM), the charged-current weak interaction links the top quark with a down-type quark with an amplitude proportional to the Cabibbo-Kobayashi-Maskawa (CKM) matrix  $V_{tq}$  ( $q = d, s, b$ ). At hadron colliders, this interaction leads to a single top quark final state through three possible processes: the  $s$ -channel decay of a virtual  $W$  ( $q\bar{q}' \rightarrow W^* \rightarrow t\bar{b}$ ), the  $t$ -channel exchange of a virtual  $W$  ( $bq \rightarrow tq'$  and  $b\bar{q}' \rightarrow t\bar{q}$ , also referred to as  $W$ -gluon fusion), and the associated production of a top quark and a  $W$  boson ( $bg \rightarrow tW^-$ ). Since the cross section for each of these processes is proportional to the CKM matrix element  $|V_{tb}|^2$ , a measurement of each single top quark production cross section determines  $|V_{tb}|$ . A study of spin correlations in single top quark production can be used to test the  $V - A$  structure of the top quark charged-current weak interaction. Such structure implies that the top quark should be polarized.

Among the three processes, the largest cross section at both the Tevatron proton-antiproton collider at Fermilab and the proton-proton Large Hadron Collider (LHC) at CERN is due to the  $t$ -channel. The next largest cross section is from the  $s$ -channel at the Tevatron, and from associated production at the LHC. The  $s$ -channel production cross section is small at the LHC because it involves a quark-antiquark collision. Similarly, associated production cross section is relatively large at the LHC because the gluon parton distribution functions (PDF) grow more rapidly with decreasing  $x$  than the light quark PDF. The  $s$ -channel and  $t$ -channel processes should be observed for the first time in Run II at the Tevatron; whereas the observation of associated production will likely have to await the LHC.

Single top quark production is also a very important background to many searches for new physics. For example, the  $s$ -channel process is a significant background to Higgs searches at the Tevatron in the production process  $q\bar{q}' \rightarrow WH$  with decay  $H \rightarrow b\bar{b}$  [1, 2, 3] and other new physics searches [4]. At the LHC, the  $Wt$  associated production is an important background to Higgs searches in the decay channel  $H \rightarrow WW$  [5] and the primary charged Higgs boson production channel  $bg \rightarrow tH^\pm$  with  $H^\pm \rightarrow \tau\nu$  [6]. As the largest single top process, the  $t$ -channel production is an important background to many new physics searches.

In Tevatron Run I, searches for single top quark production were performed by both the  $D\bar{O}$  [7] and CDF collaborations [8]. At the 95% confidence level, the  $D\bar{O}$  limit on the  $s$ -

channel production is 17 picobarn (pb) and the CDF limit is 18 pb. At the same confidence level, the  $D\bar{O}$  limit on the  $t$ -channel production cross section is 22 pb and the CDF limit is 13 pb. Searches for single top quark production in Run II have begun, and the limits from CDF are 13.6 pb in the  $s$ -channel and 10.1 pb in the  $t$ -channel [9]. The  $s$ -channel and  $t$ -channel single top quark processes can be probed separately at the Tevatron by taking advantage of  $b$ -quark tagging using displaced vertices and differences in the kinematic distributions of the  $b$ -tagged and non- $b$ -tagged jets. Usually, only one  $b$ -tagged jet can be expected in the  $t$ -channel case while two  $b$ -tagged jets can be expected in the  $s$ -channel case. This is because the  $\bar{b}$  quark produced with the top quark tends to be collinear with the initial state gluon in the  $t$ -channel, giving it a large pseudo-rapidity ( $\eta$ ) and low transverse momentum ( $p_T$ ) and thus making it challenging to  $b$ -tag this jet experimentally. It is important to separate the two processes since they have different systematic uncertainties and different sensitivities to new physics [10].

The extraction of a signal is more challenging for single top quark production than for top pair production since there are fewer objects in the final state and the overall event properties are less distinct from the large  $W$ +jets background. Therefore, an accurate calculation including higher order quantum chromodynamics (QCD) corrections is needed. The next-to-leading order (NLO)  $O(\alpha_s)$  corrections to single top quark production have already been carried out in Refs. [11, 12], which shows an uncertainty on the total cross section of about 5% by varying the factorization and renormalization scales. For the  $s$ -channel, multiple soft gluon resummation effects have been calculated [13]. In order to confront theory with experimental data, where kinematical cuts are necessary in order to detect a signal, it is crucial to accurately model event topologies of single top quark events. For this, Refs. [14, 15] have calculated the differential cross sections for on-shell single top quark production. The complete NLO calculations including both the single top quark production and decay have been done independently by two groups recently [16, 17, 18]. In both calculations, the narrow width approximation was adopted in order to link top quark production with its consequent decay [16, 17]. In Ref. [16], various kinematics distributions are examined both with and without top quark decay at NLO. In our previous study [18], we presented a detailed phenomenological analysis of  $s$ -channel single top quark production at the Tevatron, focusing on signal cross sections and kinematical distributions. To complete our study of single top processes at the Tevatron, we will focus on the single top quark

production process with the largest production cross section in this paper, namely the  $t$ -channel. A more realistic study which disentangles the signal of single top quark events from copious backgrounds and further separates the  $s$ -channel from the  $t$ -channel will be given in the future.

The paper is organized as follows. In Sec. II, we first present the inclusive cross section for the  $t$ -channel single top process using both the fixed mass narrow width approximation and the “modified” narrow width approximation. We then investigate its dependence on the top quark mass as well as the renormalization and factorization scales. In Sec. III, we examine the acceptance of single top quark events for various sets of kinematic cuts. In Sec. IV, we explore the kinematical information in the final state objects. Section V contains our conclusions.

## II. CROSS SECTION (INCLUSIVE RATE)

In order to accurately measure  $V_{tb}$  using the single top process, the uncertainties in the theoretical prediction need to be minimized. In this section, we show the inclusive production rates and discuss their dependence on the factorization and renormalization scales and the top quark mass.

We present numerical results for the production of single top quark events considering the leptonic decay of the  $W$ -boson from the top quark decay at the upgraded Tevatron (a 1.96 TeV  $p\bar{p}$  collider). Unless otherwise specified, we use the NLO parton distribution function (PDF) set CTEQ6M [19], defined in the  $\overline{MS}$  scheme, and the NLO (2-loop) running coupling  $\alpha_s$  with  $\Lambda_{\overline{MS}}$  provided by the PDFs. For the CTEQ6M PDFs,  $\Lambda_{\overline{MS}}^{(4)} = 0.326$  GeV for four active quark flavors. The values of the relevant electroweak parameters are:  $\alpha = 1/137.0359895$ ,  $G_\mu = 1.16637 \times 10^{-5} \text{ GeV}^{-2}$ ,  $M_W = 80.40$  GeV,  $M_Z = 91.1867$  GeV, and  $\sin^2 \theta_W = 0.231$  [20]. The square of the weak gauge coupling is  $g^2 = 4\sqrt{2}M_W^2 G_\mu$ . As in the  $s$ -channel study [18], here we also focus our attention only on the positively charged electron (i.e., positron), though our analysis procedure also applies to the muon final state. Including  $O(\alpha_s)$  corrections to  $W \rightarrow \bar{q}q'$ , the decay branching ratio of the  $W$  boson into leptons is  $Br(W \rightarrow \ell^+\nu) = 0.108$  [20]. Unless otherwise specified, we will choose the top quark mass to be  $m_t = 178$  GeV [21, 22] and the renormalization scale ( $\mu_R$ ) as well as the factorization scale ( $\mu_F$ ) to be equal to the top quark mass. The top quark mass and scale

dependencies of the  $t$ -channel production cross section are investigated in this section.

### A. Theoretical Cutoff Dependence

The NLO QCD differential cross sections are calculated using the one-cutoff phase space slicing (PSS) method [23, 24]. This procedure introduces a theoretical cutoff parameter ( $s_{min}$ ) in order to isolate soft and collinear singularities associated with real gluon emission subprocesses by partitioning the phase space into soft, collinear and hard regions such that

$$|\mathcal{M}^r|^2 = |\mathcal{M}^r|_{\text{soft}}^2 + |\mathcal{M}^r|_{\text{collinear}}^2 + |\mathcal{M}^r|_{\text{hard}}^2 . \quad (1)$$

In the soft and collinear regions the cross section is proportional to the Born-level cross section. Using dimensional regularization, we can evaluate the real gluon emission diagrams in  $n$ -dimensions under the soft gluon approximation in the soft region, or the collinear approximation in the collinear region, and can integrate out the corresponding phase space volume analytically. The resulting divergences are cancelled by virtual corrections or absorbed into the perturbative parton distribution functions in the factorization procedure. Since the cutoff is introduced in the calculation only for this technical reason and is unrelated to any physical quantity, the inclusive rate must not depend on it. In other words, the sum of all contributions, virtual, resolved, and unresolved corrections must be independent of  $s_{min}$ . This is the case as long as  $s_{min}$  is small enough so that the soft and collinear approximations are valid. However, numerical cancellation in the Monte Carlo (MC) integration becomes unstable if  $s_{min}$  is too small. Furthermore, the jet-finding algorithm and other infrared-safe experimental observables should also be defined in a way such that they are consistent with the choice of  $s_{min}$ . In practice, one wants to choose the largest  $s_{min}$  possible within these constraints in order to minimize the processing time of the MC integration program. For our study, we found a value of  $s_{min} = 1 \text{ GeV}^2$  to be appropriate for studying the  $t$ -channel single top process. For comparison, in Ref. [18], we found that a value of  $s_{min} = 5 \text{ GeV}^2$  is adequate for studying the  $s$ -channel single top process. A detailed discussion of the phase space slicing method can be found in Ref. [17].

Figure 1 illustrates that the total  $t$ -channel production cross section is indeed insensitive to  $s_{min}$  for a large range of  $s_{min}$  values. The figure shows the sum of the virtual and unresolved real corrections ( $s+v$ ) as well as the resolved contribution (real) to the  $t$ -channel

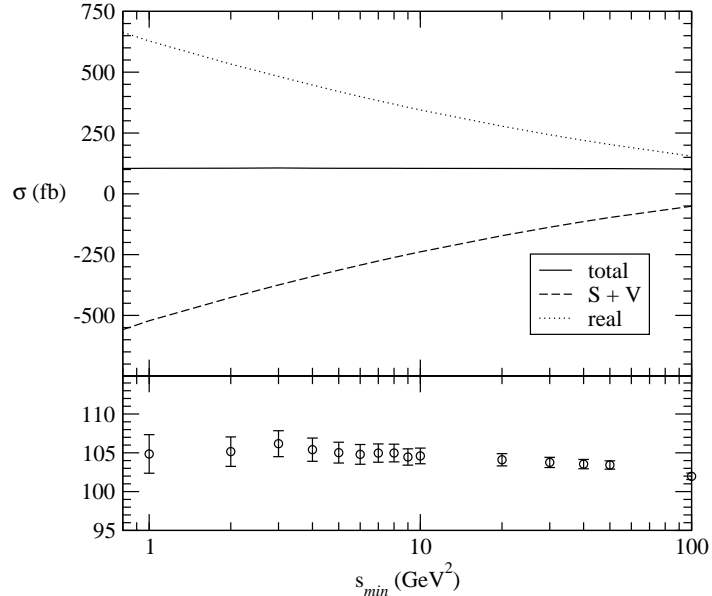


FIG. 1: The theoretical cutoff  $s_{min}$  dependence of the inclusive  $t$ -channel single top quark cross section at the Tevatron with  $\mu_R = \mu_F = m_t$  for  $m_t = 178$  GeV. The decay branching ratio  $t \rightarrow bW^+(\rightarrow e^+\nu)$  has been included.

single top process as a function of  $s_{min}$ . Although contributions from the individual pieces vary, their sum (total) remains essentially constant for a large range of  $s_{min}$ . With the choices of  $\mu_R = \mu_F = m_t$  at the Tevatron, we obtain an inclusive cross section for the  $t$ -channel single top ( $t$  only) processes (with  $W$ -boson decay branching ratio) of 104.8 femtobarn (fb), which agrees with Ref. [16].

## B. Inclusive Cross Section

To facilitate the calculation, we divided the higher-order QCD corrections into three separate gauge invariant sets: corrections from the light quark line of top quark production (LIGHT), corrections from the heavy quark line of top quark production (HEAVY), and corrections from the top quark decay (TDEC). The explicit diagrams and definitions for these three sets can be found in Ref. [17]. The inclusive cross section as well as the individual  $O(\alpha_s)$  contributions are listed in Table I. The effects of the finite widths of the top quark and  $W$ -boson have been included. As one expects, the dominant  $O(\alpha_s)$  corrections come from the heavy quark line, because the bulk part of the radiative corrections originating from the light quark line have been absorbed into the definition of the light quark PDFs.

	Cross Section (fb)	Fraction of NLO (%)
Born -level	99.2	94.6
$O(\alpha_s)$ HEAVY	5.56	5.31
$O(\alpha_s)$ LIGHT	1.03	0.98
$O(\alpha_s)$ TDEC	-0.81	-0.77
$O(\alpha_s)$ sum	5.54	5.28
NLO	104.8	

TABLE I: Inclusive  $t$ -channel single top production cross section for different subprocesses, including the top quark decay branching ratio  $t \rightarrow bW^+(\rightarrow e^+\nu)$ .

For the same reason pointed out in our previous paper [18], the TDEC contribution is very small compared to the other two.

### C. Top Quark Mass and Renormalization/Factorization Scale Dependence

In order to test the SM and measure the CKM matrix element  $V_{tb}$ , one needs an accurate prediction of single top quark production and decay so as to reduce the theoretical uncertainties. Besides the top quark mass, the choices of renormalization and factorization scales also contribute to the uncertainty of the theoretical prediction. The renormalization scale  $\mu_R$  is introduced when redefining the bare parameters in terms of the renormalized parameters, while the factorization scale  $\mu_F$  is introduced when absorbing the collinear divergences into parton distribution functions. Therefore, both  $\mu_R$  and  $\mu_F$  are unphysical and the final predictions should not depend on them. However, since we work at a fixed order in perturbation theory, we indeed see a dependence of the predicted cross section on  $\mu_R$  and  $\mu_F$ . The change due to varying the scale is formally of higher order. Since the single top quark rate is small at the Tevatron, it is important to reduce the scale uncertainty in order to compare the theory prediction with experimental data. Here, we examine the top quark mass and the scale dependence of the  $t$ -channel production cross section.

As shown in Fig. 2, the cross section changes by about  $\pm 9\%$  when the top quark mass  $m_t$  is varied by its current uncertainty of about  $\mp 5$  GeV around 178 GeV. It can also be seen

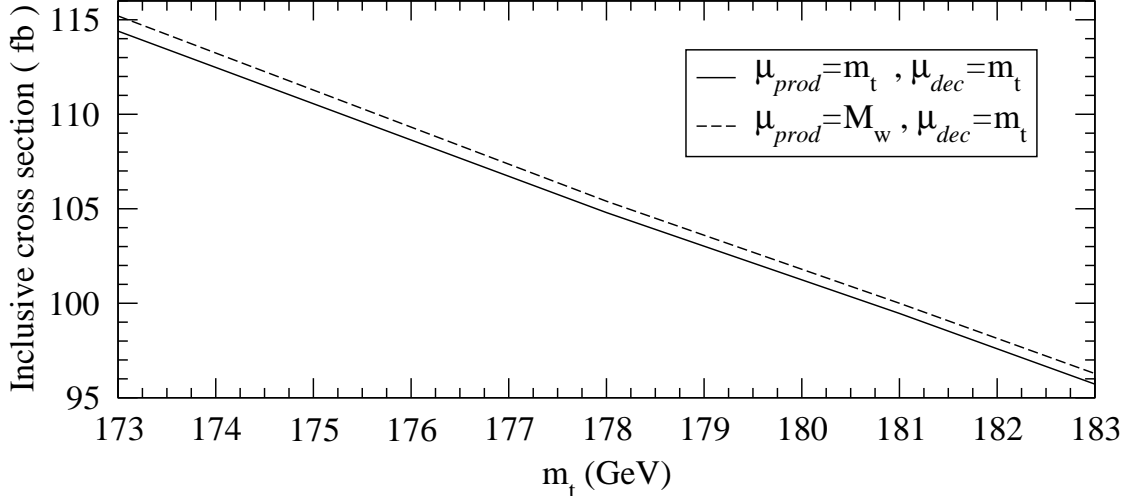


FIG. 2: Top quark mass dependence as well as renormalization and factorization scale dependence of the inclusive  $t$ -channel single top quark cross section at the Tevatron. The decay branching ratio of  $t \rightarrow bW^+(\rightarrow e^+\nu)$  has been included.

that measuring the top quark mass to an uncertainty of 1–2 GeV will reduce the theoretical uncertainty on the single top cross section correspondingly. The reduction in uncertainty on the  $t$ -channel single top production rate will improve the measurement of the CKM matrix  $V_{tb}$ .

In order to examine the scale dependence of the  $t$ -channel single top production rate, we show in Fig. 2 the results of two typical scales: one is the top quark mass ( $\mu_F = \mu_R^{prod} = m_t$ ), shown as the solid line, the other is the  $W$  boson mass ( $\mu_F = \mu_R^{prod} = M_W$ ), shown as the dashed line. For the decay of top quark, we take  $\mu_R^{dec} = m_t$ , which gives similar results as the choice of  $\mu_R^{dec} = M_W$ . The band constrained by these two  $\mu_F$  scales represents a range of uncertainty due to the NLO predictions. The usual practice for estimating the yet-to-be calculated higher order QCD correction to a perturbative cross section is to vary around the typical scale by a factor of 2, though in principle the “best” scale to be used for estimation cannot be determined without completing the higher order calculation. In Fig. 3 we show the total cross section of the  $t$ -channel single top production for a range of the scale  $\mu_F$  which, for simplicity, is set to be equal to  $\mu_R$ . We have multiplied the LO cross sections by a constant factor (the “K-factor”) of 1.04 (shown as the dashed line) in order to compare to the NLO ones (shown as the solid-line). It is clear that the NLO calculation reduces the scale dependence. For example, when the scale is changed from  $\mu_F/2$  to  $2\mu_F$  around



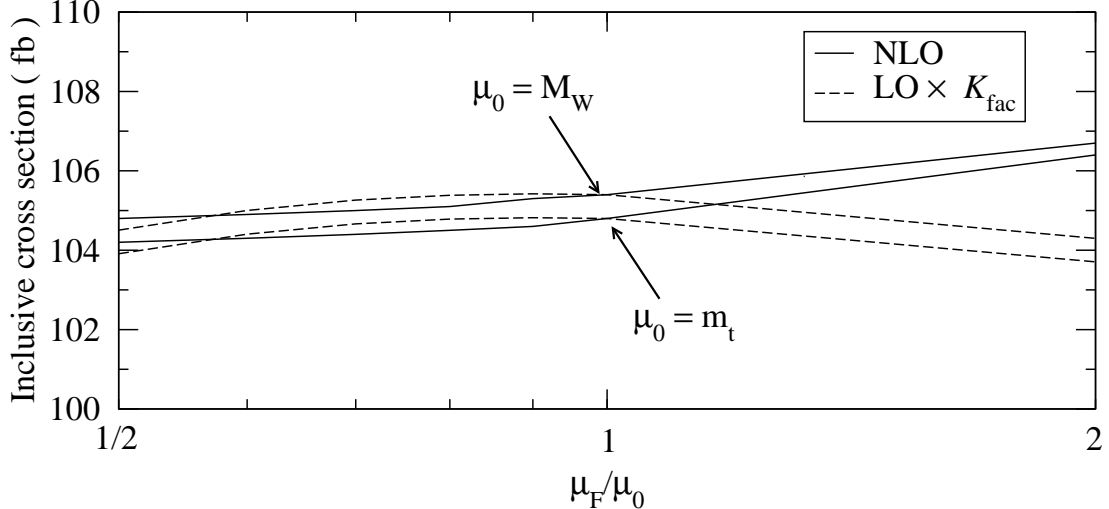


FIG. 3: Inclusive  $t$ -channel single top quark production cross section at the Tevatron for  $m_t = 178$  GeV, versus the ratio of the factorization scale  $\mu_F$  to its typical value  $\mu_0$ , where  $\mu_0 = m_t$  (solid line) and  $\mu_0 = M_W$  (dashed line), respectively. The decay branching ratio of  $t \rightarrow bW^+(\rightarrow e^+\nu)$  has been included.

$\mu_F = m_t$ , the LO rate varies by  $-0.9\%$  to  $-1.0\%$  while the NLO rate varies only by  $-0.6\%$  to  $+1.3\%$ . Similar results also hold for varying the scale around  $\mu_F = M_W$ .

### III. SINGLE TOP ACCEPTANCE STUDIES

In this section we explore the final state objects of  $t$ -channel single top quark events. Although the  $W$ -boson from the top quark decay can decay in both leptonic and hadronic modes, we focus only on the leptonic decay mode in this study because the all-jet production mode of single top quark events is difficult to observe experimentally. Therefore, the signature of  $t$ -channel single top quark events which is accessible experimentally consists of one charged lepton, missing transverse energy, together with two or three jets. Since we are studying the effects of NLO QCD radiative corrections on the production rate and the kinematic distributions of single top quark events at the parton level in this paper, we do not include any detector effects, such as jet energy resolution or  $b$ -tagging efficiency. Only an approximation of kinematic acceptances of a generic detector are considered. Since the Tevatron is  $p\bar{p}$  collider, and  $p\bar{p}$  is a CP-even state, the production cross sections for  $b\bar{t}(j)$  at the Tevatron are the same as those for  $t\bar{b}(j)$  (when ignoring the small CP violation effect

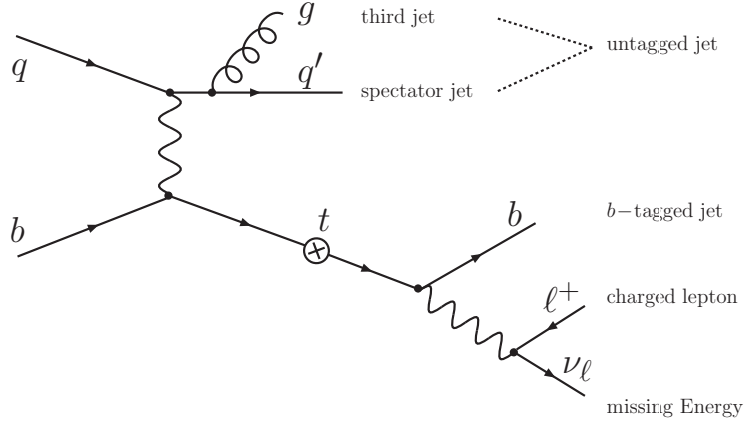


FIG. 4: Pictorial illustration of the notation used in this paper.

induced by the CKM mixing matrix in quarks). For simplicity we therefore only consider distributions of  $t$ -channel single top quark events in this work in which a  $t$  quark (not including  $\bar{t}$ ) decays into  $W^+(\rightarrow \ell^+\nu)$  and a  $b$  quark. In this section, we first present the event topology of the  $t$ -channel single top process, and then introduce a jet finding algorithm and the various kinematical cuts in order to study the acceptance.

### A. Event Topology

At tree level, the collider signature of the  $t$ -channel single top process includes two jets (one  $b$ -tagged jet from the  $b$  quark from the top quark decay, and one non- $b$ -tagged jet from the light quark), one charged lepton, and missing transverse energy ( $\cancel{E}_T$ ) in the final state. This signature becomes more complicated beyond tree level, as Fig. 4 indicates. The light quark jet is also called “spectator jet”, and the label “untagged jet” refers to all jets which do not contain a  $b$  or  $\bar{b}$  quark.

At NLO, besides the charged lepton and  $\cancel{E}_T$ , there may be two jets (one  $b$ -tagged jet and one untagged jet) as for the Born-level, or there may be three jets. The flavor composition of the three-jet final state depends on the origin of the third jet. When it is a gluon or anti-quark (cases (a-c) in Fig. 5), there is one  $b$ -tagged jet and two untagged jets. When it is a  $\bar{b}$  quark (case (d) in Fig. 5, also called  $W$ -gluon fusion), there are two  $b$ -tagged jets and one untagged jet. Therefore, prescriptions are needed to identify the  $b$  jet from the top quark decay and the light quark jet produced with the top quark.

In our study, we differentiate the following three cases:

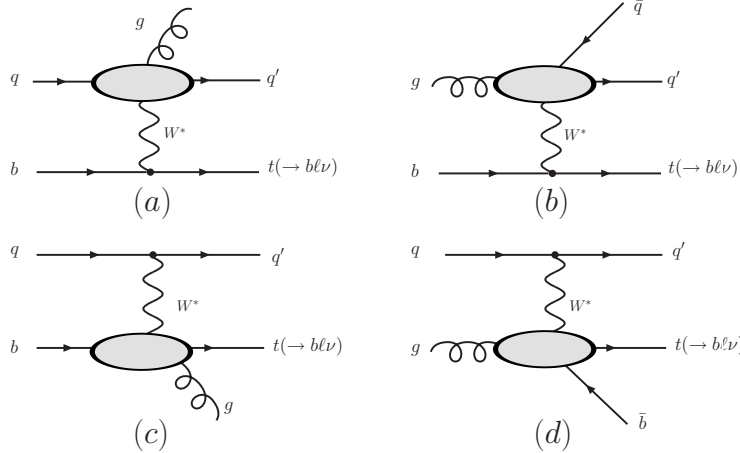


FIG. 5: Representative diagrams of the real emission corrections for the  $t$ -channel single top process: (a) and (b) represent the real radiative corrections to the LIGHT quark line, while (c) and (d) represent the real radiative corrections to the HEAVY quark line. The NLO QCD corrections are indicated by the large shaded ellipse. Detailed Feynman diagrams can be found in Ref. [17].

1. Born-level-type exclusive two-jet events (containing the  $b$  quark and the light quark):  
In Born-level type events, i.e. without an additional hard jet, the final state is given by the  $b$  jet from the top quark decay and the light quark jet produced with the top quark. Experimentally, this configuration is easily reconstructed because the  $b$ -tagged jet is identified as the  $b$  quark, and the untagged jet is assigned to the spectator jet. We note that in our phenomenology study to be presented in Sec. IV we shall concentrate on inclusive two-jet events and exclusive three-jet events.
2. Exclusive three-jet events with one  $b$  jet (containing the  $b$  quark, the light quark, and a gluon or anti-quark):

When the radiated gluon is reconstructed as a separate jet in the LIGHT, TDEC, or HEAVY corrections, the final state contains one  $b$  jet and two other jets. As shown later, the transverse momentum and energy differences can be used to separate the spectator jet from the gluon jet (third jet). The transverse momentum of the spectator jet, which comes from the initial quark ( $q$ ) after emitting the effective  $W$ -boson, peaks around  $\sim M_W/2$ , thus its energy is large. In comparison, the transverse momentum of the gluon jet is small. Due to the collinear enhancement, the resolved gluon jet prefers to move along the beam line direction at smaller transverse momentum ( $p_T$ ) for both

the LIGHT and HEAVY corrections, and along the  $b$  quark moving direction for the TDEC correction.

3. Exclusive three-jet events with one  $b$  jet and one  $\bar{b}$  jet (containing the  $b$  quark, the light quark, and a  $\bar{b}$  quark):

This final state is produced in the  $W$ -gluon fusion process, case (d) of Fig. 5. In this case, the spectator jet can be uniquely identified, but the  $b$  jet from the top decay cannot because heavy flavor tagging algorithms do not distinguish  $b$  jets from  $\bar{b}$  jets experimentally. Although the likelihood of tagging two  $b$ -jets is smaller than that of tagging a single  $b$ -jet, requiring two  $b$ -tagged jets will suppress the QCD and  $W$ +jets backgrounds significantly. We again can use transverse momentum differences to separate  $b$  jets from  $\bar{b}$  jets. The  $b$  jet from the top quark decay has a transverse momentum peaking around  $m_t/3$ , while the  $\bar{b}$  jet from gluon splitting tends to move along the beam line (the gluon-moving direction) due to the collinear enhancement and is much softer. These kinematic differences also enable us to separate the  $t$ -channel process from the  $s$ -channel process, recalling that in the  $s$ -channel process, both the  $b$  jet and the  $\bar{b}$  jet are preferentially produced at central rapidity and large  $p_T$ .

The unique signature of the  $t$ -channel single top process is the spectator jet in the forward direction, which can help to suppress the copious backgrounds, such as  $Wb\bar{b}$  and  $t\bar{t}$  production. Studying the kinematics of this spectator jet is important in order to have a better prediction of the acceptance of  $t$ -channel single top quark events and of the distribution of several important kinematic variables. In this work, we study the impact of the NLO QCD corrections on the kinematic properties of the spectator jet. As pointed out in Ref. [25], in the effective- $W$  approximation, a high-energy  $t$ -channel single top quark event is dominated by a longitudinal  $W$  boson and the  $b$  quark fusion diagram. It is the same effective longitudinal  $W$  boson that dominates the production of a heavy Higgs boson at high energy colliders via the  $W$ -boson fusion process. For a heavy SM Higgs boson, the longitudinal  $W$  boson fusion process dominates the Higgs boson production rate. Therefore, it is also important to study the kinematics of the spectator jet in  $t$ -channel single top quark events in order to have a better prediction for the kinematics of Higgs boson events via the  $WW$  fusion process, i.e.  $q\bar{q}(WW) \rightarrow Hq'\bar{q}'$  at hadron colliders.

## B. Acceptance

In order to meaningfully discuss the effects of gluon radiation in single top quark events, we must define a jet as an infrared-safe observable. In this study, we adopt the cone-jet algorithm [26] as explained in our previous work [18]. More specifically, we adopt the  $E$ -scheme cone-jet approach (4-momenta of particles in a cone are simply added to form a jet) with radius  $R = \sqrt{\Delta\eta^2 + \Delta\phi^2}$  in order to define  $b$ ,  $q$  and possibly extra  $g$ ,  $\bar{q}$ , or  $\bar{b}$  jets, where  $\Delta\eta$  and  $\Delta\phi$  are the separation of particles in the pseudo-rapidity  $\eta$  and the azimuthal angle  $\phi$ , respectively. For reference, we shall consider both  $R = 0.5$  and  $R = 1.0$ . The same  $R$ -separation will also be applied to the separation between the lepton and each jet.

The kinematic cuts imposed on the final state objects are:

$$\begin{aligned}
 P_T^\ell &\geq 15 \text{ GeV} \quad , \quad |\eta_\ell| \leq \eta_\ell^{max} \quad , \\
 \cancel{E}_T &\geq 15 \text{ GeV} \quad , \\
 E_T^j &\geq 15 \text{ GeV} \quad , \quad |\eta_j| \leq \eta_j^{max} \quad , \\
 \Delta R_{\ell j} &\geq R_{cut} \quad , \quad \Delta R_{jj} \geq R_{cut} \quad ,
 \end{aligned}
 \tag{2}$$

where the jet cuts are applied to both the  $b$ - and light quark jets as well as any gluon or antiquark jet in the final state. Two lepton pseudo-rapidity cuts are considered here: a loose version with  $\eta_\ell^{max} = 2.5$  and a tight version with  $\eta_\ell^{max} = 1.0$ . Similarly, loose and tight cuts are also considered for the jet pseudo-rapidity,  $\eta_j^{max} = 3.0$  and  $\eta_j^{max} = 2.0$ , respectively. The minimum transverse energy cuts on the lepton as well as the jets is 15 GeV. Each event is furthermore required to have at least one lepton and two jets passing all selection criteria. The cut on the separation in  $R$  between the lepton and the jets as well as between different jets is given by  $R_{cut}$  which is chosen to be 0.5 (or 1.0).

In Table II, we show the single top production cross sections in fb for the loose and tight set of cuts listed in Eq. (2) for the different subprocesses. A larger value for  $R_{cut}$  reduces the acceptance significantly mainly because more events fail the lepton-jet separation cut. While this is only a 13% reduction at the Born-level, the difference grows to 25% at NLO. Hence, a smaller cone size is preferred in order to keep the acceptance at a high level. For events with at least three jets, imposing a harder cut on the transverse momentum of each jet ( $E_{Tj} > 30 \text{ GeV}$ ) decreases the contribution from the LIGHT and HEAVY corrections by a factor of 3 to 4, but the contribution from the TDEC correction by more than a factor

$\sigma$ [fb]		LO	NLO	Heavy	Light	Decay
Tevatron (a)	$tq + tqj$	65.6	64.0	4.9	-3.4	-0.59
	$tq + tqj, E_{Tj} > 30 \text{ GeV}$	46.3	44.0	4.2	-3.3	-1.7
	$tqj$		25.3	15.5	5.1	4.8
	$tqj, E_{Tj} > 30 \text{ GeV}$		7.4	5.4	1.3	0.75
Tevatron (b)	$tq + tqj$	56.8	48.1	-0.45	-4.4	-2.2
	$tq + tqj, E_{Tj} > 30 \text{ GeV}$	40.1	33.3	0.0	-3.3	-2.1
	$tqj$		14.8	10.8	2.2	1.7
	$tqj, E_{Tj} > 30 \text{ GeV}$		4.5	3.7	0.58	0.20
Tevatron (c)	$tq + tqj$	31.1	34.0	5.8	-2.8	0.82
	$tq + tqj, E_{Tj} > 30 \text{ GeV}$	24.4	24.2	3.8	-2.7	-0.7
	$tqj$		11.4	6.7	2.4	2.3
	$tqj, E_{Tj} > 30 \text{ GeV}$		3.9	2.8	0.74	0.41

TABLE II: The  $t$ -channel single top production cross section at the Tevatron (in fb ) for different subprocesses under various cut scenarios: (a) is the loose version with  $\eta_l^{max} = 2.5$ ,  $\eta_j^{max} = 3.0$ , and  $R_{cut} = 0.5$ , (b) is the loose version with a larger jet clustering cone size (and jet-lepton separation cut) of  $R_{cut} = 1.0$ , and (c) is the tight version of cuts with  $\eta_l^{max} = 1.0$ ,  $\eta_j^{max} = 2.0$ , and  $R_{cut} = 0.5$ . The first two columns show the Born-level and full NLO cross sections, the last three columns show the contributions from the different  $O(\alpha_s)$  processes. The decay branching ratio  $t \rightarrow bW(\rightarrow e\nu)$  is included.

6. This large reduction occurs because the top quark mass sets the scale for the top quark decay contribution rather than the invariant mass of  $tq'$  system, resulting in a softer jet  $E_T$  spectrum for the TDEC correction (cf. Fig. 24, to be discussed in Sec. IV D).

Figure 6 shows how the observed cross section changes as a function of the jet  $E_T$  cut when applying the loose set of cuts, including a requirement of there being at least two jets in the event. The figure also shows the dependence of the fraction of two-jet events and three-jet events on the jet  $E_T$  cut. At the Born-level, there are only two-jet events, whereas  $O(\alpha_s)$  corrections can produce an additional soft jet. The fraction of events with these additional jets is low only for very high jet  $E_T$  thresholds. For typical jet  $E_T$  thresholds

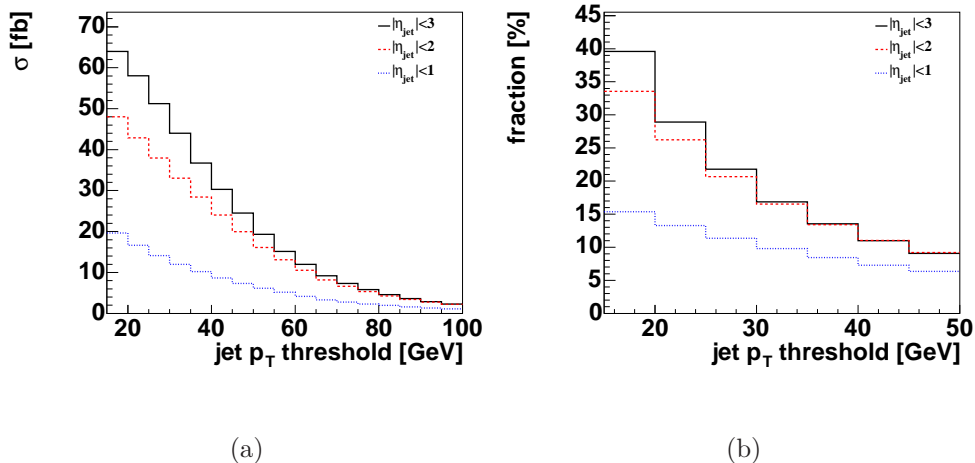


FIG. 6: Cross section and fraction of three-jet events at NLO for varying jet  $p_T$  cuts, requiring only that  $n_{jets} \geq 2$ , and not making any cuts on the electron or neutrino. Shown is the total cross section for events with two or three jets as a function of the jet  $E_T$  cut for three different jet pseudo-rapidity cuts (a) and the fraction of three-jet events as a function of the jet  $p_T$  for different jet pseudo-rapidity cuts (b). The lowest threshold considered is 15 GeV.

considered by experiments of 15 GeV to 25 GeV these jets add a significant contribution. As expected, the effect is not quite as large when only jets within a very small  $\eta$  range are considered because the extra jet typically has higher  $\eta$ . In order to study  $O(\alpha_s)$  effects it is thus important to set the jet  $\eta$  cut as high as possible and the jet  $E_T$  cut as low as possible.

As mentioned before, the event rate for single top quark events is small and it is important for experiments to maximize their acceptance. We will thus use the loose set of cut values for the following discussion:  $\eta_l^{max} = 2.5$ ,  $\eta_j^{max} = 3.0$ , and  $R_{cut} = 0.5$ ,  $E_{Tj}^{min} = 15$  GeV, cf. Eq. (2).

#### IV. SINGLE TOP QUARK EVENT DISTRIBUTIONS

In this section we examine the kinematic properties of single top quark events. As discussed in the previous section, the signature of the  $t$ -channel process includes at least one  $b$ -tagged jet, one untagged jet, one charged lepton, and missing energy. At the Born-level, it is straightforward to identify the single top final state using the  $b$ -tagged jet and the reconstructed  $W$  boson to reconstruct the top quark and identifying the spectator jet as

the light quark. At NLO, however, an additional jet is radiated, which will complicate the reconstruction of the top quark final state. First, this is because the additional jet can be either a  $b$ -tagged jet or an untagged jet. When it is the  $b$ -tagged jet, we need to select the correct  $b$  quark from the two possible jets in the final state to reconstruct the top quark. When it is the untagged jet, we need to select the correct spectator jet. Second, the additional untagged jet can come from either the production or the decay of the top quark. Production-stage emission occurs before the top quark goes on shell and decay-stage emission occurs only after the top quark goes on shell. In production emission events, the  $W$  boson and  $b$  quark momenta will combine to give the top quark momentum, while in the decay emission event the gluon momentum must also be included in order to reconstruct the top quark momentum properly. To find the best prescription for identifying the correct  $b$  jet and spectator jet, we first examine various kinematic distributions of the final state particles. We then investigate two top quark reconstruction prescriptions: using the leading  $b$ -tagged jet and the best jet algorithm. Choosing the  $b$ -tagged jet prescription, we can also improve the reconstruction efficiency for the  $W$  boson. We then study the effects of NLO corrections on distributions concerning the reconstructed top quark, in particular spin correlations between the final state particles. Finally, we explore the impact of the radiated jet in exclusive three-jets events. We use only the loose set of cuts to maximize the efficiency when examining the distributions and efficiencies in detail.

## A. Final State Object Distributions

### 1. Charged Lepton and Missing Transverse Energy

In this section we examine various kinematic distributions of final state objects after event reconstruction and after applying the loose set of cuts, cf. Table I and Eq. (2). We concentrate on inclusive two-jet events in this section because they give more reliable infrared-safe predictions.

Figures 7 (a) and (c) show the transverse momentum of the electron and the missing transverse energy  $\cancel{E}_T$ , respectively. As expected, because they are leptons and not quarks, the change in shape when going from Born-level to NLO is not very large for the electron or the missing transverse energy. The pseudo-rapidity distribution of the electron is given in



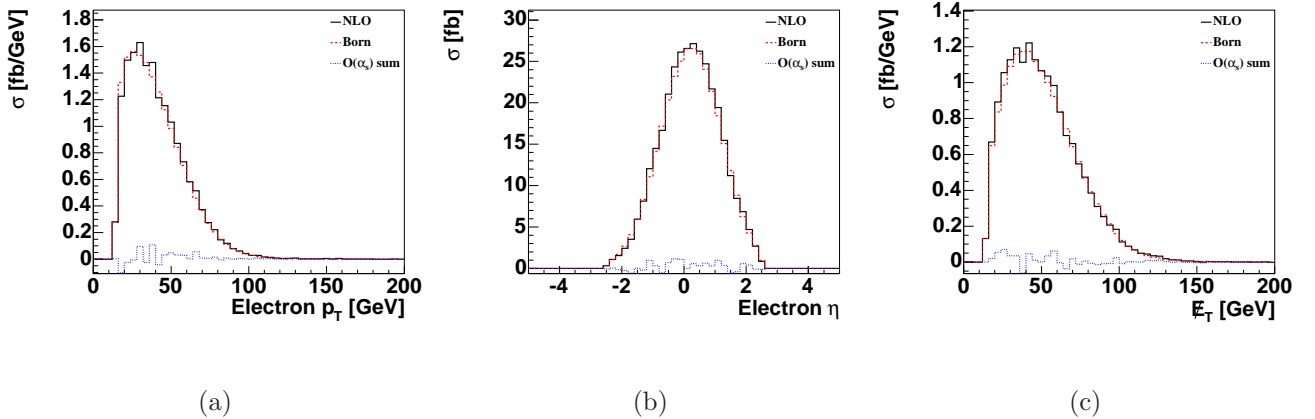


FIG. 7: The transverse momentum  $p_T$  (a) and pseudo-rapidity  $\eta$  (b) distributions of the electron and the missing transverse energy  $E_T$  (c) after selection cuts, comparing Born-level to  $O(\alpha_s)$  corrections.

Fig. 7(b). This distribution widens at NLO, but again the effect is small because the overall  $O(\alpha_s)$  contribution to the event rate is small, cf. Table I. We note that the peak position of the  $E_T$  distribution is at a higher value than that of the electron  $p_T$  because the neutrino from the  $W$ -boson decay moves preferentially along the direction of the top quark. This is due to the left-handed nature of the charged current interaction and can easily be seen when examining the spin correlations between the charged lepton and the top quark in the top quark rest frame. We will comment more on this subject in Sec. IV C.

## 2. Spectator Jet

The differences between the  $s$ -channel and  $t$ -channel single top processes at the Born-level are that the former has two  $b$ -taggable jets in the final state (the  $b$  quark and the  $\bar{b}$  quark) while the latter only has one  $b$ -taggable jet and also has one light quark jet. This untagged jet (spectator jet) is a unique feature of the  $t$ -channel process which can be used to disentangle  $t$ -channel single top quark events from the copious backgrounds. Therefore, its kinematic distributions need to be well studied, especially the impact of  $O(\alpha_s)$  corrections on the features which make this jet a unique signature, such as the spectator jet pseudo-rapidity, cf. Fig. 8.

The pseudo-rapidity distribution of the spectator jet is asymmetric because the Tevatron

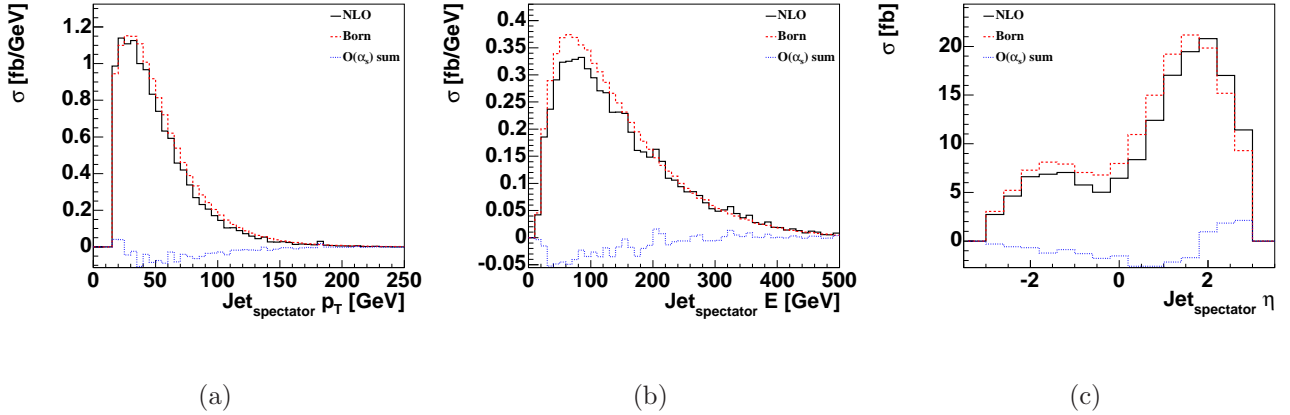


FIG. 8: Transverse momentum  $p_T$  (a), energy  $E$  (b) and the pseudo-rapidity  $\eta$  (c) of the spectator jet after selection cuts, comparing Born-level to  $O(\alpha_s)$  corrections.

is a  $p\bar{p}$  collider [25]. In order to produce a heavy top quark decaying to a positively charged lepton, the valence quark from the proton is most important, implying that the light quark will tend to move in the proton direction. We define the positive  $z$ -direction to be the proton direction in the laboratory frame, thus the pseudo-rapidity of the spectator jet will tend to be positive. Similarly, the spectator jet in an anti-top quark event produced from the  $t$ -channel process will preferably be at a negative pseudo-rapidity due to the large anti-up quark parton distribution inside the antiproton. The  $O(\alpha_s)$  corrections shift the spectator jet to even more forward pseudo-rapidities due to additional gluon radiation. However, since the  $O(\alpha_s)$  corrections are small compared to the Born-level contribution, the spectator jet pseudo-rapidity distribution only shifts slightly. As Fig. 9 shows, the LIGHT and HEAVY contributions have almost opposite behavior. The former shifts the spectator jet to even higher pseudo-rapidities, while the latter shifts it more to the central rapidity region. This behavior is due to two different effects, as illustrated in Fig. 9 (b), in which “PA” denotes that the light quarks come from the proton while the bottom quarks from the anti-proton and vice versa for “AP”. After separating the contributions by whether the light quark is from the proton or the antiproton, it can be seen that the HEAVY corrections shift the proton contribution down and the antiproton contribution up due to the slight change in acceptance caused by the additional jet. The LIGHT corrections show the opposite tendency. For the TDEC contribution, all corrections have similar shapes and the sum of them leaves the spectator jet pseudo-rapidity unchanged, as expected. After summing the negative soft-

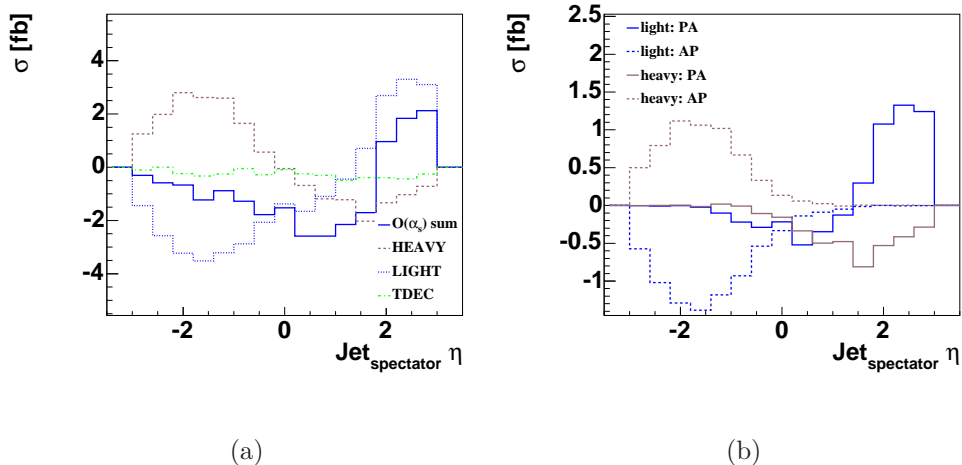


FIG. 9: Each individual contribution of the  $O(\alpha_s)$  corrections to the spectator jet pseudo-rapidity, summed (a), separately for the case when the incoming up-type quark is from the proton and anti-proton (b). Here, “PA” and “AP” denotes the initial state light quark originating from proton and anti-proton, respectively.

plus-virtual corrections with the real emission corrections, we obtain the result shown in Fig. 8, which shows that the  $O(\alpha_s)$  correction shifts the spectator jet to be in even more forward direction.

Besides its forward rapidity, the spectator jet also has large transverse momentum. Since it comes from the initial state quark after emitting the effective  $W$  boson, the transverse momentum peaks around  $\sim M_W/2$ , cf. Fig. 8. By comparison, the third jet is most often much softer, we can thus use  $p_T$  of the jet to identify the the spectator jet when considering exclusive three-jet events.

### 3. $b$ Jet

Compared to the lepton and  $\cancel{E}_T$ , the effects of the  $O(\alpha_s)$  corrections on the reconstructed  $b$  jet are more pronounced. Figure 10 shows a comparison of the  $b$  jet  $p_T$  distribution between the Born-level and  $O(\alpha_s)$  corrections. The  $p_T$  distribution of the  $b$  jet is predominantly determined by the top quark mass and therefore peaks at  $\sim m_t/3$ . The NLO QCD corrections broaden the transverse momentum distribution and shift the peak position to lower values. The location of the mean of the distributions depends on the cuts that are applied because

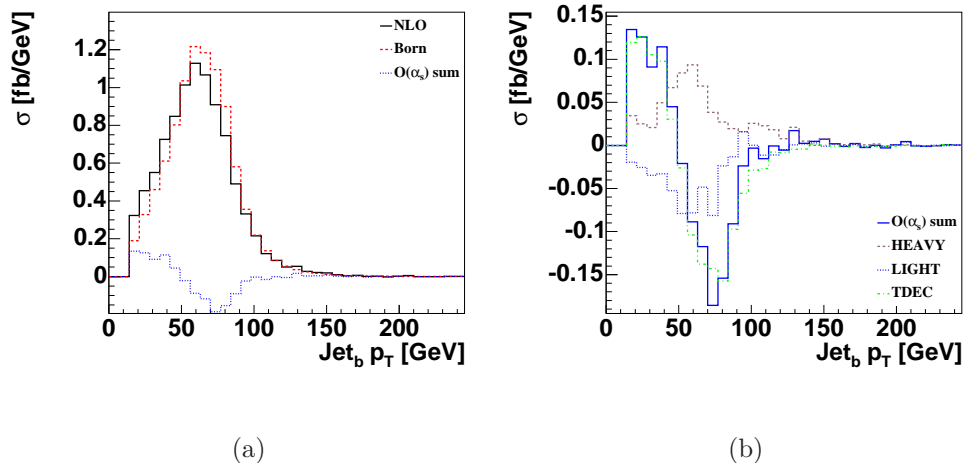


FIG. 10: Transverse momentum  $p_T$  of the  $b$  jet after selection cuts, comparing Born-level to  $O(\alpha_s)$  corrections (a) and the individual  $O(\alpha_s)$  contributions (b).

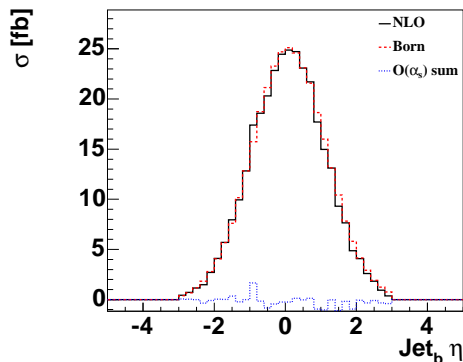


FIG. 11: Pseudo-rapidity  $\eta$  of the  $b$ -jet after selection cuts, comparing Born level to  $O(\alpha_s)$  corrections.

the different  $O(\alpha_s)$  corrections have different effects: in the case of the loose cuts it increases from 64 GeV at the Born-level to 62 GeV at full NLO. The LIGHT corrections shift the mean of the  $b$  jet  $p_T$  distribution up, the HEAVY corrections leave it mostly unchanged, and the TDEC corrections tend to shift it down. The  $b$  jet  $p_T$  distribution receives a large contribution from the TDEC corrections, as expected. When a gluon is radiated from the top quark decay, it tends to move along the  $b$  jet direction due to collinear enhancements and therefore shifts the  $b$  jet  $p_T$  distribution to the small  $p_T$  region, as shown in Fig. 10.

The  $b$  jet pseudo-rapidity distribution is less affected by the  $O(\alpha_s)$  corrections, as can be seen in Fig. 11. The top quark is so heavy that it is mostly produced in the central rapidity

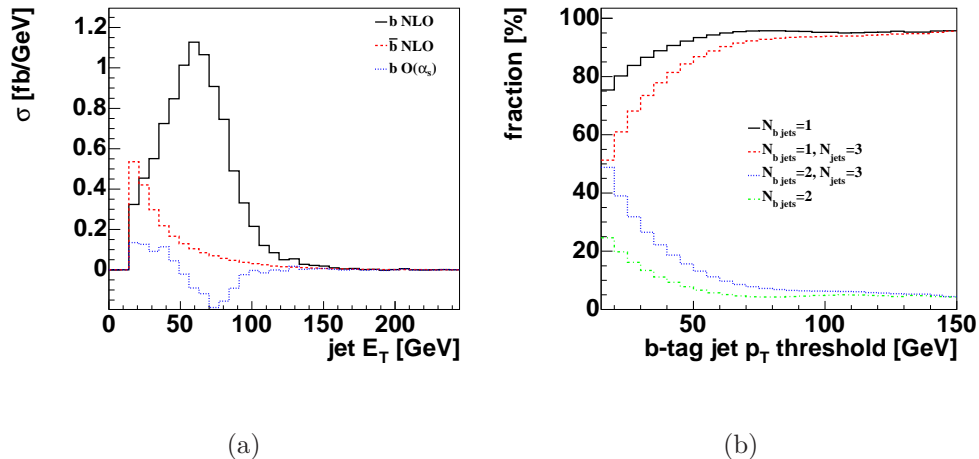


FIG. 12: Momentum of the  $b$  and  $\bar{b}$  jets (a) and fraction of events with one or two  $b$ -tagged jets as a function of the jet  $p_T$  threshold, for both inclusive two-jet and exclusive three-jet events (b).

region and thus the  $b$  jet from its decay also peaks around a pseudo-rapidity of zero. The shape of the  $b$  jet pseudo-rapidity distribution remains almost unchanged compared to the Born-level because it comes from the top quark decay.

Figure 12 compares the momentum of the  $b$  jet and the  $\bar{b}$  jet at NLO and examines the fraction of events containing one or two  $b$ -tagged jets in the final state. Events with both  $b$  and  $\bar{b}$  jets originate from the  $W$ -gluon fusion subprocess,  $qg \rightarrow q'\bar{b}t(\rightarrow bW(\rightarrow \ell^+\nu))$ . While the fraction of events with two  $b$ -tagged jets is high for low jet  $p_T$ , it drops quickly. For a jet  $p_T$  above 50 GeV, the fraction of events with both  $b$  and  $\bar{b}$  jets is less than 5%. Figure 12 also shows that for exclusive three-jet events, the fraction of events with two  $b$ -tagged jets is much higher. About half of the events contain two  $b$ -tagged jets for the lowest threshold of 15 GeV, and the fraction only goes down to 5% when the jet  $p_T$  reaches about 140 GeV.

#### 4. $H_T$ Distribution

The impact that different  $O(\alpha_s)$  corrections have on the  $p_T$  of the jets is also reflected in event-wide energy variables such as the total transverse energy in the event ( $H_T$ ), defined as

$$H_T = p_T^{\text{lepton}} + \cancel{E}_T + \sum_{\text{jets}} p_T^{\text{jet}}. \quad (3)$$

The distribution of  $H_T$  for  $t$ -channel single top quark events is shown in Fig. 13. The Born-

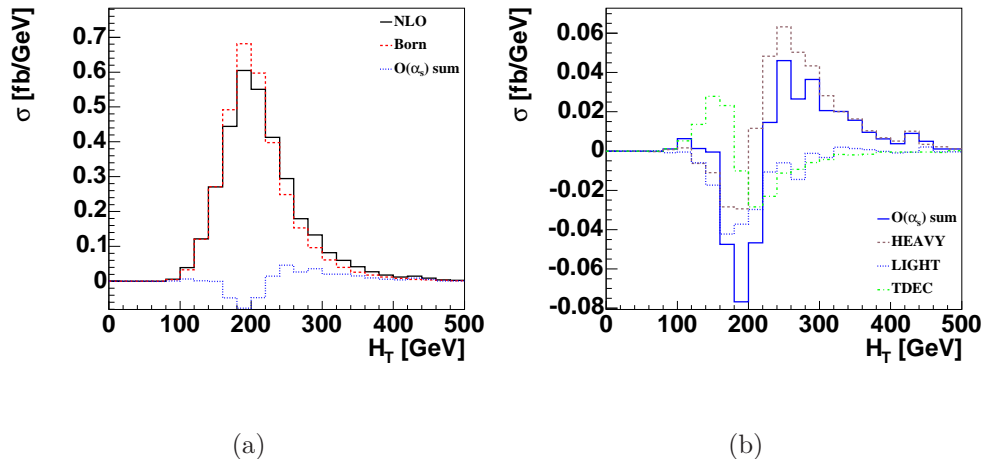


FIG. 13: Total event transverse energy  $H_T$  after selection cuts, comparing Born level to  $O(\alpha_s)$  corrections (a) and the individual  $O(\alpha_s)$  contributions (b).

level  $H_T$  distribution peaks around 200 GeV. Both the HEAVY and LIGHT contributions decrease the height of the peak and shift it to higher values, and all three  $O(\alpha_s)$  contributions broaden the distribution.

## B. Event Reconstruction

When analyzing single top quark events we would like to take advantage not only of simple single-object kinematics but also of correlations between objects. In order to take full advantage of the correlations, we need to reconstruct the event completely, not just the final state jets but also intermediate particles, in particular the  $W$ -boson and the top quark.

The  $W$  boson can be reconstructed from the final state electron and the observed missing transverse energy,  $\cancel{E}_T$ . The lack of information about the beam-direction component of the neutrino momentum ( $p_z^\nu$ ) that would prevent this reconstruction is typically overcome by requiring that the invariant mass of the electron-neutrino system be equal to the mass of the  $W$  boson. This additional constraint results in two possible solutions for  $p_z^\nu$ . One usually follows the prescription given in Ref. [27] of choosing the solution which has the smaller  $|p_z^\nu|$ . This picks the correct  $p_z^\nu$  in about 70% of the events. The price paid for this method is that the  $W$  boson will blur the spin correlation in the reconstructed single top quark event. We will see later that we can improve on this by using a top mass constraint.

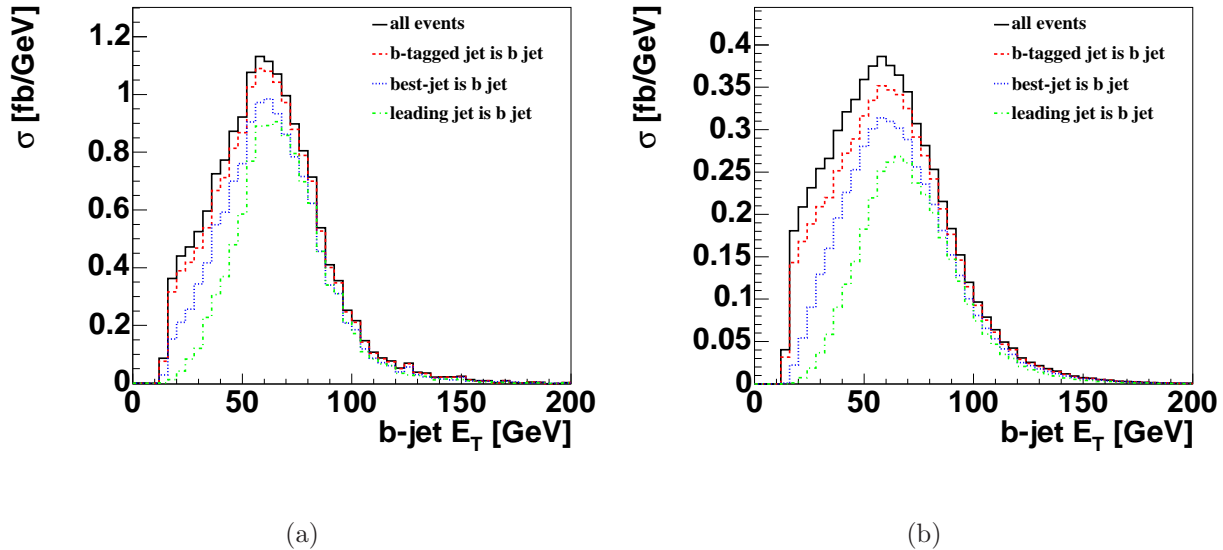


FIG. 14: Transverse momentum of the  $b$  quark jet, for all events (solid histogram), only for those events for which the leading  $b$ -tagged jet corresponds to the  $b$  quark jet (dashed histogram), only for those events in which the best jet corresponds to the  $b$  quark jet (dotted histogram), and only for those events in which the leading jet corresponds to the  $b$  quark jet (dash-dotted histogram). The transverse momentum is shown for the inclusive two-jet sample (a) and for the exclusive three-jet sample (b).

In order to reconstruct the top quark, the reconstructed  $W$  boson then needs to be combined with the  $b$  jet from the top quark decay. The challenge to overcome here is the proper identification of the  $b$  jet. In the  $s$ -channel single top process, we used the “best-jet” algorithm to find the correct  $b$  jet among the two possible  $b$ -tagged jets in the final state, making use of the known top quark mass ( $m_t = 178$  GeV) [18]. The effectiveness of the best-jet algorithm is mainly limited by the efficiency of the  $W$  boson identification method; if the  $W$  boson is not reconstructed properly, then identifying the  $b$  jet from the top quark decay becomes a random choice.

Unlike the  $s$ -channel processes, inclusive two-jet events of the  $t$ -channel single top processes typically only contain one  $b$ -tagged jet in the final state, corresponding to the  $b$  quark from the top quark decay. Figure 14 shows a comparison of three different algorithms to identify the  $b$  jet from the top quark decay: a) using the leading jet (highest  $p_T$ ) in the event, b) using the leading  $b$ -tagged jet in the event, and c) using the best jet. The leading jet in

this case could be either the  $b$  jet or the light quark jet, thus the efficiency for identifying the  $b$ -jet from top quark decay with method a) is rather low. The leading  $b$ -tagged jet is either the  $b$  jet from the top quark decay or the  $\bar{b}$  jet originating from the  $W$ -gluon fusion subprocess. Figure 14 shows that the leading  $b$ -tagged jet corresponds to the  $b$  quark from the top decay most of the time; it identifies the  $b$  quark correctly in 95% of the events in the inclusive sample after the loose selection cuts. We expect the efficiency to drop in the three-jet sample because of the additional  $\bar{b}$  quark in the final state. However, as shown in Fig. 12, the  $b$  jet from the top quark decay is much harder than the  $\bar{b}$  jet radiated from the initial state gluon. As a result, the leading  $b$ -tagged jet corresponds to the  $b$  quark from the top quark decay in 90% of the exclusive three-jet events. Figure 14 shows that this fraction is slightly smaller for low  $b$  jet  $p_T$  values, and reaches 100% above about 100 GeV. By comparison, the best jet corresponds to the  $b$  quark in only 80% of the events in the inclusive sample and about 72% of the events in the exclusive three-jet sample. We therefore choose the method of identifying the leading  $b$ -tagged jet as the  $b$  quark from the top decay. Having identified the  $b$  quark in this manner with no additional assumptions allows us to use it to reconstruct the top quark and the  $W$  boson more accurately, in particular to determine the longitudinal momentum of the neutrino ( $p_z^\nu$ ). We reconstruct the  $W$  boson as above using a  $W$  mass constraint. We then identify the proper neutrino  $p_z^\nu$  by choosing the solution for which the invariant mass of the reconstructed  $W$  and the leading  $b$ -tagged jet is closest to the true top quark mass, i.e. 178 GeV.

This method identifies the correct neutrino  $p_z^\nu$  about 92% of the time at the Born-level and about 84% of the time at NLO. These efficiencies are slightly smaller than the  $b$  quark identification efficiencies shown in Fig. 14 due to the finite widths of the  $W$  boson and the top quark.

Figure 15 shows the invariant mass of the reconstructed top quark, comparing the different methods to identify the  $b$  quark and the  $W$  boson from the top quark decay. The top quark width is larger than it would be at parton level even though no kinematic smearing was applied in this study to mimic the detector effect. This is the result of using the reconstructed kinematics of the  $W$  boson (in particular the neutrino  $z$ -momentum) rather than parton level information. Furthermore, since the same reconstructed  $W$  boson was used for all curves in Fig. 15, differences among the individual curves are solely due to the jet choice used to reconstruct the top quark. Finally, because parton level information is



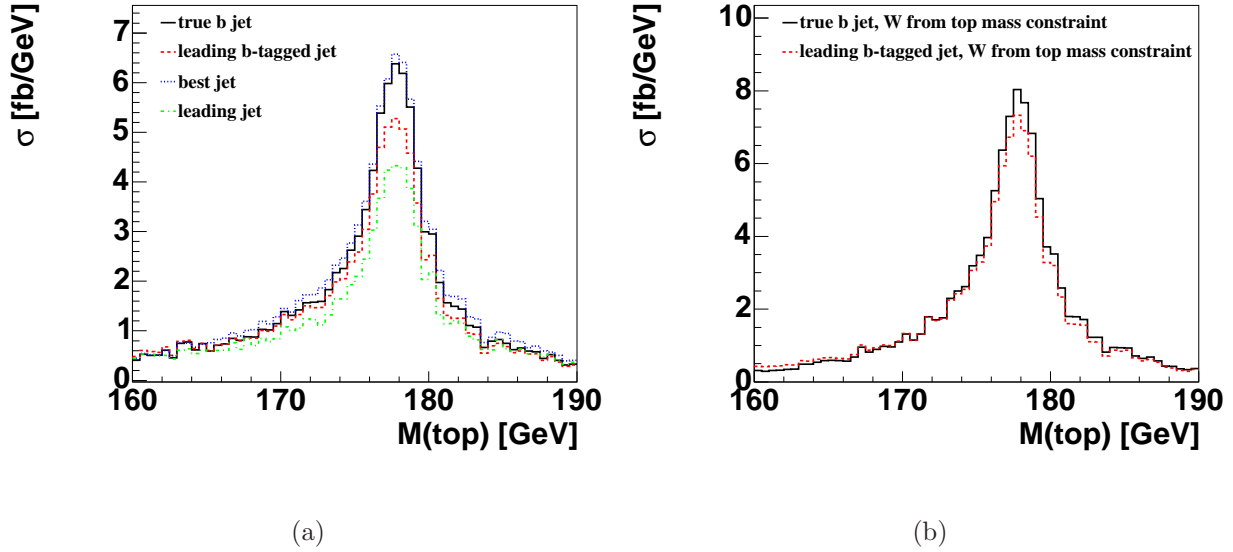


FIG. 15: Invariant mass of the reconstructed  $W$  and a jet object. This jet object is: the jet containing the  $b$  quark from the top decay, using parton information (solid line), the leading  $b$ -tagged jet (dashed line), the best jet (dotted line), or the leading jet (dot-dashed line). The  $W$  is reconstructed either using the standard neutrino  $p'_z$  constraint (a) or a top mass constraint (b).

used for the  $b$  jet curve, it functions as a reference and upper limit for the other methods.

Figure 15(a) shows the top mass reconstructed with the  $W$  boson using the standard method of choosing the smaller  $|p'_z|$ . As expected, using the leading jet gives the worst performance, and using the leading  $b$ -tagged is a better choice. Given this choice for the neutrino, however, the best jet algorithm looks best because for those cases where the neutrino has been misreconstructed, the best jet algorithm sometimes chooses the wrong jet and thus it falsely appears to give well reconstructed top mass because the algorithm chooses an invariant mass close to 178 GeV. Figure 15(b) shows the top mass reconstructed with the  $W$  boson reconstructed from a top mass constraint. The overall height of the mass peak is higher in Fig. 15(b) than in Fig. 15(a), indicating that this method is able to reconstruct the  $W$  boson and  $b$  jet correctly more often. It can also be seen that for this choice of  $W$  boson reconstruction, we can properly reconstruct the true top quark with the leading  $b$ -tagged jet with very high efficiency. Using the leading  $b$ -tagged jet together with a top mass constraint to reconstruct the  $W$  boson gives the best reconstructed top quark and is the most efficient event reconstruction algorithm for  $t$ -channel single top quark events. We will henceforth

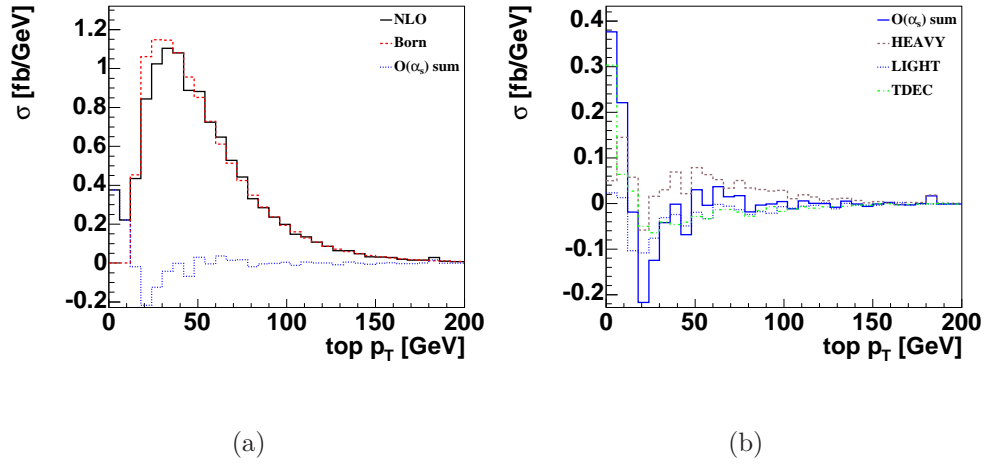


FIG. 16: Transverse momentum of the reconstructed top quark, comparing Born-level to  $O(\alpha_s)$  corrections(a) and the individual  $O(\alpha_s)$  contributions (b).

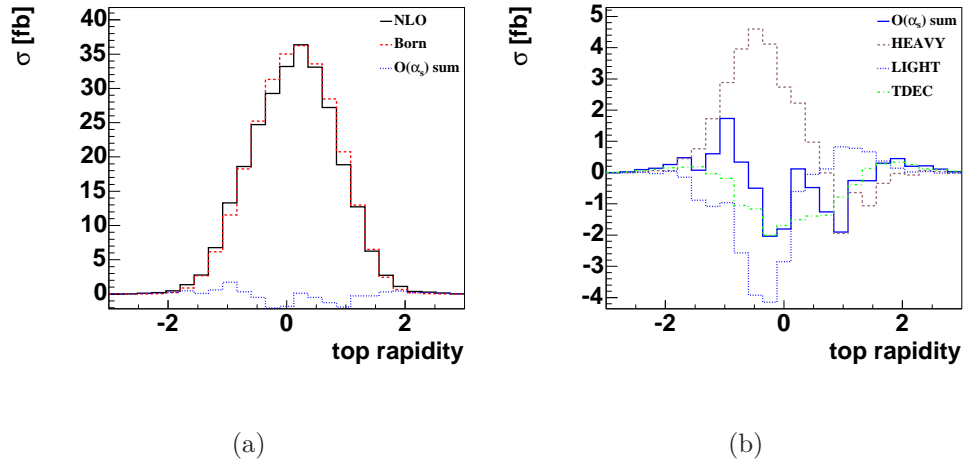


FIG. 17: Rapidity of the reconstructed top quark, comparing Born-level to  $O(\alpha_s)$  corrections(a) and the individual  $O(\alpha_s)$  contributions (b).

focus on this algorithm.

Figure 16 shows the transverse momentum of the top quark reconstructed from the leading  $b$ -tagged jet together with the top mass constraint to reconstruct the  $W$  boson, hence, to determine  $p_z'$ . The LIGHT and HEAVY corrections tend to shift the top quark  $p_T$  to higher values, while the TDEC correction lowers it as expected. The different  $O(\alpha_s)$  corrections have only a small effect on the top quark rapidity shown in Fig. 17, similar to the  $b$  jet

above. The HEAVY correction tends to shift the top quark to negative rapidities, while the LIGHT correction tends to shift it to positive rapidities, resulting in a net effect of only a small change in rapidity.

### C. Top Quark Polarization

Having identified the  $b$  jet from the top quark decay and the  $W$  boson, we can now study correlations expected from event kinematics. As noted in the previous section, we shall focus on the study of top quark polarization using the leading  $b$ -tagged jet and the top mass constraint for the  $W$  boson, because it reconstructs the final state correctly with the highest efficiency.

In the SM, the top quark produced in single top quark events is highly polarized, and this polarization can in principle be measured. The top quark is by far the heaviest known fermion and the only known fermion with a mass at the electroweak symmetry-breaking scale. Thus, it is hoped that a detailed study of top quark coupling to other particles will be of great utility in determining if the SM mechanism for electroweak symmetry-breaking is the correct one, or if new physics is responsible [28]. Angular correlations among the decay products of polarized top quarks provide a useful handle on these couplings. It has been pointed out that among the decay products of the top quark, the charged lepton is maximally correlated with the top quark spin [29, 30]. We can thus obtain the most distinctive distribution by plotting the angle between the charged lepton and the spin axis of the top quark in its rest frame.

Although the top quark is produced via the left-handed charged current, there is no reason to believe that the helicity basis will give the best description of the top quark spin. Choosing an appropriate basis could maximize spin correlation effects. Three polarization bases have been studied in the literature for the  $t$ -channel process, and they differ by the reference frame used to define the polarization: the helicity basis, the beamline basis, and the so-called “spectator” basis [31]. All three work in the top quark rest frame, but they have different reference axis for the top quark spin, cf. Fig. 18. In the more commonly used helicity basis, the top quark spin is measured along the top quark direction of motion in the center of mass frame which is chosen as the frame of the (reconstructed top quark, spectator jet) system after event reconstruction. In the beamline basis, the top quark spin

is measured along the incoming proton direction. In the spectator basis we can maximize spin correlations by taking advantage of the fact that the top quark produced through the  $t$ -channel single top processes is almost 100% polarized along the direction of the spectator quark. In the discussion below, we will examine the polarization of single top quark events in these three bases.

In helicity basis, the c.m. frame needs to be reconstructed in order to define the top quark momentum. Due to additional jet radiation, the determination of the c.m. frame at NLO is more complicated than at the Born-level. The additional radiation will also blur the spin correlation, therefore, choosing the appropriate frame will reduce this effect. In this study, two options for reconstructing the c.m. frame are investigated:

1.  $tq(j)$ -frame: the c.m. frame of the incoming partons. This is the rest frame of all the final state objects (reconstructed top quark and all others jets). In exclusive two-jet events, this frame is the same as the c.m. frame at the Born-level, i.e. reconstructed from summing over momentum of the top quark and spectator jet. In exclusive three-jet events, this frame is reconstructed by summing over the 4-momenta of top quark, spectator jet, and the third-jet from our parton level calculation.
2.  $tq$ -frame: the c.m. frame of the top quark and spectator jet. In this case, even in exclusive three-jet events, the reference frame is constructed by summing over only the 4-momenta of the top quark and spectator jet. Note that this differs from the  $tq(j)$ -frame only in exclusive three-jet events.

As shown in Table III and discussed below, the degree of top polarization is larger in the  $tq$ -frame than in the  $tq(j)$ -frame. Therefore, in the figures below we only display the top quark polarization in the  $tq$ -frame.

In the helicity basis, the polarization of the top quark is examined as the angular distribution ( $\cos\theta_{hel}$ ) of the lepton in the c.m. frame relative to the moving direction of the top quark in the same frame. The angular correlation in this frame is given by

$$\cos\theta_{hel} = \frac{\vec{p}_t \cdot \vec{p}_\ell^*}{|\vec{p}_t||\vec{p}_\ell^*|}, \quad (4)$$

where  $\vec{p}_\ell^*$  is the charged lepton three-momentum defined in the rest frame of the top quark, whose three momentum is denoted as  $\vec{p}_t$ , which is in turn defined in the c.m. frame. For a

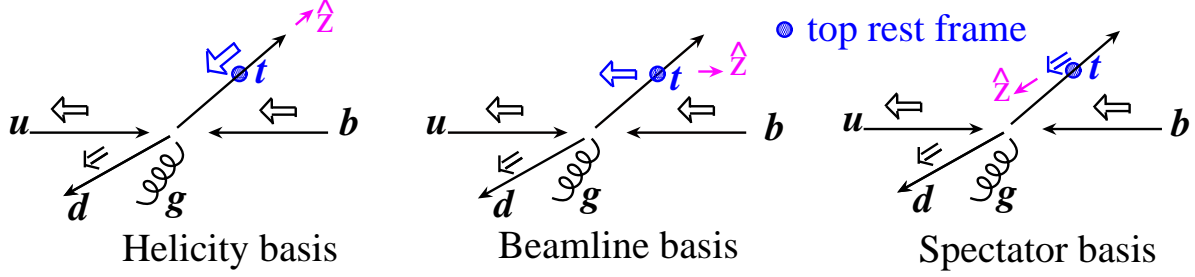


FIG. 18: Illustration of the three choices for the top quark spin basis. The circle denotes the top quark rest frame and the blue arrows denote the top quark spin direction.

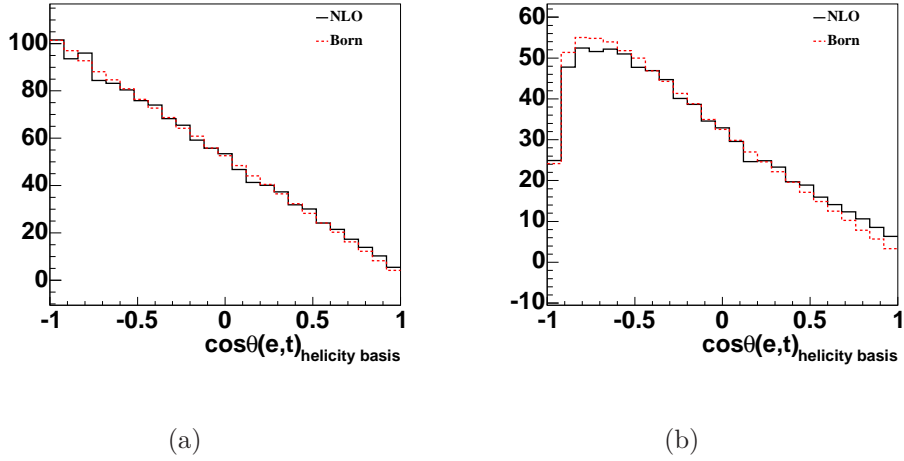


FIG. 19: Top quark polarization in the helicity basis using the full parton information (a) and after event reconstruction with selection cuts (b), comparing Born-level to  $O(\alpha_s)$  corrections. The Born-level and NLO curves have been normalized to the same area.

left-handed top quark, the angular correlation of the lepton  $\ell^+$  is given by  $(1 - \cos \theta_{hel})/2$ , and for a right-handed top quark, it is  $(1 + \cos \theta_{hel})/2$ . Figure 19(a) shows that this linear relationship for  $\cos \theta_{hel}$  is indeed a valid description for  $t$ -channel single top quark events at the parton level. The figure also shows that the top quark is not completely polarized in the helicity basis, and that this polarization is only slightly weakened when including  $O(\alpha_s)$  corrections. Figure 19 (b) shows that this weakening is amplified after event reconstruction, where the effect of the lepton-jet separation cut can also be seen, as a drop-off of the  $\cos \theta_{hel}$  distribution close to a value of  $-1$ .

In the “spectator” basis, the relevant angular correlation for the  $t$ -channel process is

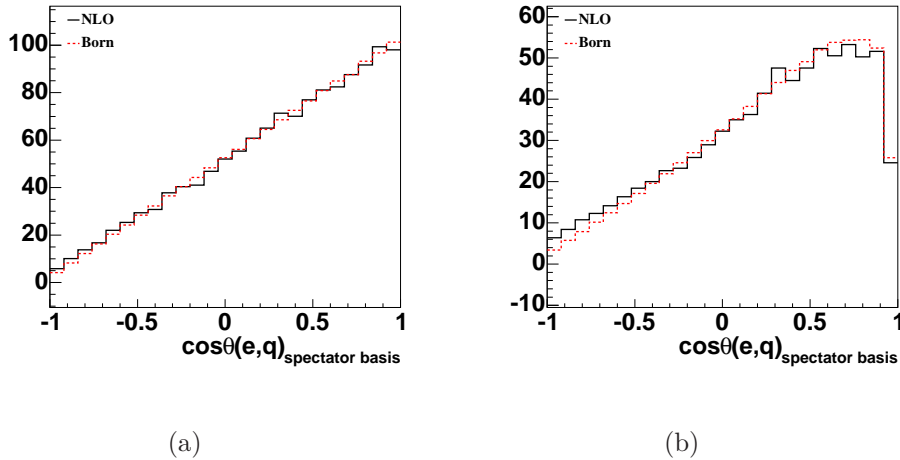


FIG. 20: Top quark polarization in the spectator basis using the full parton information (a) and after event reconstruction with selection cuts (b), comparing Born-level to  $O(\alpha_s)$  corrections. The Born-level and NLO curves have been normalized to the same area.

$\cos \theta_{spec}$ , defined as

$$\cos \theta_{spec} = \frac{\vec{p}_{spec}^* \cdot \vec{p}_\ell^*}{|\vec{p}_{spec}^*| |\vec{p}_\ell^*|}, \quad (5)$$

where  $\vec{p}_{spec}^*$  is the spectator jet three-momentum in the top quark rest frame and  $\vec{p}_\ell^*$  is the lepton three-momentum in the top quark rest frame. Although this basis picks the wrong spin axis direction for the  $\bar{d}b$  and  $b\bar{d}$  initial states, it is correct most of the time at the Tevatron collider. This is because the Tevatron is a  $p\bar{p}$  collider which means that the production rate of  $p\bar{p}(ub, bu) \rightarrow dt$  is much larger than  $p\bar{p}(\bar{d}b) \rightarrow \bar{u}t$ . The large slope found in Fig. 20 shows that the spectator basis indeed results in a large degree of correlation for  $t$ -channel single top quark events at the parton level. The slope shown in Fig. 20(a) is opposite to that in Fig. 19(a) due to the fact that the spin quantization axis points in opposite directions for the two basis, cf. Fig. 18. The degree of polarization of the top quark is larger than that in the helicity basis, and the  $O(\alpha_s)$  corrections blur the spin correlation effects only slightly, both at parton level and after event reconstruction. The reconstructed  $\cos \theta_{spec}$  distribution again shows a drop-off due to the lepton-jet separation cut, in this case at high  $\cos \theta_{spec}$ .

In the “beamline” basis, the relevant angular correlation for the  $t$ -channel process is  $\cos \theta_{beam}$ , defined as

$$\cos \theta_{beam} = \frac{\vec{p}_p^* \cdot \vec{p}_\ell^*}{|\vec{p}_p^*| |\vec{p}_\ell^*|}, \quad (6)$$

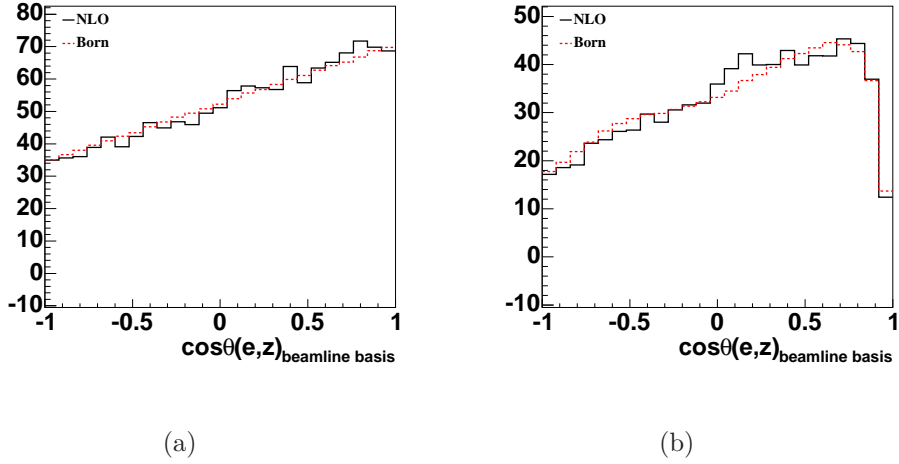


FIG. 21: Top quark polarization in the beamline basis using the full parton information (a) and after event reconstruction with selection cuts (b), comparing Born-level to  $O(\alpha_s)$  corrections. The Born-level and NLO curves have been normalized to the same area.

where  $\vec{p}_p^*$  is the proton three-momentum in the top quark rest frame and  $\vec{p}_\ell^*$  is the lepton three-momentum in the top quark rest frame. In this analysis, we orient the coordinate system such that protons travel in the positive  $z$  direction and anti-protons travel in the negative  $z$  direction. For a top quark polarized along the proton moving direction, the angular distribution of the lepton  $\ell^+$  is  $(1 + \cos \theta_{beam})/2$ , while for a top quark polarized along the anti-proton moving direction it is  $(1 - \cos \theta_{beam})/2$ . Figure 21 shows that this linear relationship for  $\cos \theta_{beam}$  is a valid description for  $t$ -channel single top quark events at the parton level. However, the top quark is less polarized in the beamline basis at parton level. In this case, the  $O(\alpha_s)$  corrections actually improve the spin correlation effects at parton level. After event reconstruction the situation is similar as before, the spin correlation is further reduced and shows a drop-off close to 1.

To better quantify the change in polarization, it is useful to define the degree of polarization  $\mathcal{D}$  of the top quark. This is given as the ratio

$$\mathcal{D} = \frac{N_- - N_+}{N_- + N_+},$$

where  $N_-$  ( $N_+$ ) is the number of left-handed (right-handed) polarized top quarks in the helicity basis. Similarly, in the spectator (beamline) basis,  $N_-$  ( $N_+$ ) is the number of top quarks with polarization against (along) the direction of the spectator jet (proton) three

momentum in the top quark rest frame. The angular distribution is then given by [32]

$$\begin{aligned} \frac{1}{\sigma} \frac{d\sigma}{d(\cos\theta)} &= \frac{N_-}{N_- + N_+} \frac{1 + \cos\theta}{2} + \frac{N_+}{N_- + N_+} \frac{1 - \cos\theta}{2} \\ &= \frac{1}{2} (1 + D \cos\theta). \end{aligned}$$

Simple algebra leads to the following identity:

$$\mathcal{D} = -3 \int_{-1}^1 x \frac{d\sigma}{\sigma dx} dx, \quad (7)$$

where  $\frac{d\sigma}{\sigma dx}$  is the normalized differential cross section as a function of the polar angle  $x$ . Here,  $x$  denotes  $\cos\theta_{hel}$  in the helicity basis, etc. Based on the degree of polarization  $\mathcal{D}$ , we can easily get the spin fractions  $\mathcal{F}_{\pm}$  as:

$$\begin{aligned} \mathcal{F}_- &= \frac{N_-}{N_- + N_+} = \frac{1 + \mathcal{D}}{2}, \\ \mathcal{F}_+ &= \frac{N_+}{N_- + N_+} = \frac{1 - \mathcal{D}}{2}. \end{aligned}$$

Note that  $\mathcal{F}_-$  ( $\mathcal{F}_+$ ) is the fraction of left-handed (right-handed) polarized top quarks in the helicity basis, etc.

We can also define the asymmetry  $\mathcal{A}$  of the distribution as

$$\mathcal{A} = \frac{\int_{-1}^0 d\sigma(\cos\theta) - \int_0^1 d\sigma(\cos\theta)}{\int_{-1}^0 d\sigma(\cos\theta) + \int_0^1 d\sigma(\cos\theta)}. \quad (8)$$

It is easy to check that without imposing any kinematic cuts,  $D = 2\mathcal{A}$ . Furthermore, the ratio of top quarks with spin along the basis direction will be  $r_{\uparrow} = 0.5 - \mathcal{A}$  when no cuts are applied. However, when cuts are imposed, these two relations break down. Table III shows that the relationship  $\mathcal{D} = 2\mathcal{A}$  indeed holds at parton level (within rounding errors) and is still approximately true at  $O(\alpha_s)$ .

In Table III, we present our results for inclusive two-jet events at the parton level before selection cuts and after the loose set of cuts and event reconstruction (cf. Sec. IV B). The result for exclusive three-jet events is shown in Table IV. For completeness, we also include the same study for the  $s$ -channel single top process in the Appendix.

- We note that in the helicity basis, the degree of top quark polarization is larger in the  $tq$ -frame than in the  $tq(j)$ -frame (the usual c.m. frame of the incoming partons) at the parton level. The degree of top quark polarization is 94% in the  $tq$ -frame and only



		$\mathcal{D}$		$\mathcal{F}$		$\mathcal{A}$	
		LO	NLO	LO	NLO	LO	NLO
Helicity basis:	Parton level ( $tq(j)$ -frame)	0.96	0.74	0.98	0.87	0.48	0.37
	Parton level ( $tq$ -frame)	0.96	0.94	0.98	0.97	0.48	0.47
	Reconstructed events ( $tq(j)$ -frame)	0.84	0.73	0.92	0.86	0.46	0.41
	Reconstructed events ( $tq$ -frame)	0.84	0.75	0.92	0.88	0.46	0.42
Spectator basis:	Parton level	-0.96	-0.94	0.98	0.98	-0.48	-0.47
	Reconstructed events	-0.85	-0.77	0.93	0.89	-0.46	-0.42
Beamline basis:	Parton level	-0.34	-0.38	0.67	0.69	-0.17	-0.19
	Reconstructed events	-0.30	-0.32	0.65	0.66	-0.17	-0.20

TABLE III: Degree of polarization  $\mathcal{D}$ , polarization fraction  $\mathcal{F}$ , and asymmetry  $\mathcal{A}$  for inclusive two-jet single top quark events, at the parton level before cuts and after selection cuts and event reconstruction, in the  $t$ -channel process. Here,  $\mathcal{F}$  corresponds to  $\mathcal{F}_-$  in the helicity basis for left-handed top quarks and to  $\mathcal{F}_+$  in the spectator and beamline bases for top quarks with polarization along the direction of the spectator-jet and proton three momentum, respectively. Also, the  $tq(j)$ -frame in the helicity basis denotes the c.m. frame of the incoming partons, while the  $tq$ -frame denotes the rest frame of the top quark and spectator jet.

74% in  $tq(j)$ -frame. This is due to the fact the degree of top quark polarization in inclusive two-jet events is a mixture of contributions from both exclusive two-jet events and exclusive three-jet events. Table IV shows that for exclusive three-jet events, the degree of top quark polarization is larger in the  $tq$ -frame than in the  $tq(j)$ -frame. This reduction in the degree of polarization for the  $tq(j)$ -frame is due to events in which the additional jet is produced before the exchange of the virtual  $W$  boson. After event reconstruction, the two frames give almost the same degree of top quark polarization.

- We find that at the parton level stage, there is very little difference between the helicity basis (using the  $tq$ -frame) and the spectator basis, and that both of them give significantly better polarization than the beamline basis both at Born-level and NLO. The top quark is almost completely polarized in the helicity and spectator bases, and the  $O(\alpha_s)$  corrections only degrade that picture slightly. The similarity between

these two bases is due to the fact that the degree of polarization of the top quark is dominated by exclusive two-jet events for which these two bases are equivalent, cf. the Born-level results in Table III. After event reconstruction for the inclusive two-jet sample, the degree of polarization is reduced as expected in both the helicity and spectator bases.

- In the beamline basis, the polarization actually increases when going from Born-level to NLO, but it is still much lower than in the other two bases. After event reconstruction, the degree of polarization is also reduced.
- In the exclusive three-jet sample, the degree of polarization is further reduced because the third-jet affects the kinematics of either spectator jet or the top quark. The helicity basis with  $tq$ -frame gives almost the same degree of polarization as the spectator basis.

Our study shows that the helicity basis (using the  $tq$ -frame) and the spectator basis are equally good to study the top quark polarization. Unlike the  $s$ -channel process in which the  $W$ -boson is not perfectly reconstructed in the best-jet algorithm and thus the polarization measurement was significantly degraded after event reconstruction, using the leading  $b$ -tagged jet and the top mass constraint gives excellent final state reconstruction in the  $t$ -channel process, and the degree of top quark polarization is only somewhat degraded after event reconstruction.

#### D. Distributions for Three-jet Events

As shown in Fig. 6, a large fraction of the events passing the loose selection cuts contain three jets. In this section we focus on the properties of these three-jet events and the additional jet.

In events containing two untagged jets, we can use the  $p_T$  of the untagged jet to pick up the spectator jet. When the  $\bar{b}$  jet from the initial state gluon splitting in the  $W$ -gluon fusion process is mistagged, it will also contribute an untagged jet to the event. For simplicity, we will assume fully efficient, perfect  $b$ -tagging here and consider events with single  $b$ -tags and double  $b$ -tags separately.

From Fig. 6 it is clear that the jet multiplicity at NLO depends strongly on the jet  $p_T$  cut. Figure 22 shows that it also depends strongly on the jet pseudo-rapidity cut. The

		$\mathcal{D}$	$\mathcal{F}$	$\mathcal{A}$
Helicity basis:	Parton level ( $tq(j)$ -frame)	0.65	0.83	0.35
	Parton level ( $tq$ -frame)	0.78	0.89	0.43
	Reconstructed events ( $tq(j)$ -frame)	0.63	0.81	0.34
	Reconstructed events ( $tq$ -frame)	0.70	0.85	0.38
Spectator basis:	Parton level	-0.78	0.89	-0.42
	Reconstructed events	-0.70	0.85	-0.38
Beamline basis:	Parton level	-0.26	0.63	-0.16
	Reconstructed events	-0.27	0.63	-0.16

TABLE IV: Degree of polarization  $\mathcal{D}$ , polarization fraction  $\mathcal{F}$ , and asymmetry  $\mathcal{A}$  for exclusive three-jet single top quark events, at parton level and after event reconstruction, in the  $t$ -channel process. Here,  $\mathcal{F}$  corresponds to  $\mathcal{F}_-$  in the helicity basis for left-handed top quarks and to  $\mathcal{F}_+$  in the spectator and beamline bases for top quarks with polarization along the direction of the spectator-jet and proton three momentum, respectively. The  $tq(j)$  frame in the helicity basis denotes the c.m. frame of the incoming partons, while the  $tq$  frame denotes the rest frame of the reconstructed top quark and light quark.

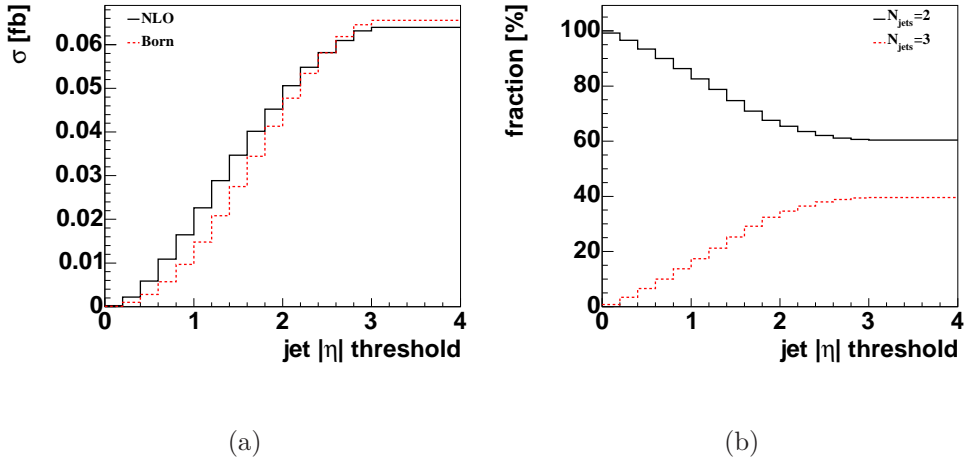


FIG. 22: Inclusive cross section and fraction of three-jet events at NLO for varying jet pseudo-rapidity cuts, after the loose selection cuts. Shown is the total cross section as a function of the jet pseudo-rapidity cut (a) and the fraction of two-jet and three-jet events as a function of the jet pseudo-rapidity cut (b).

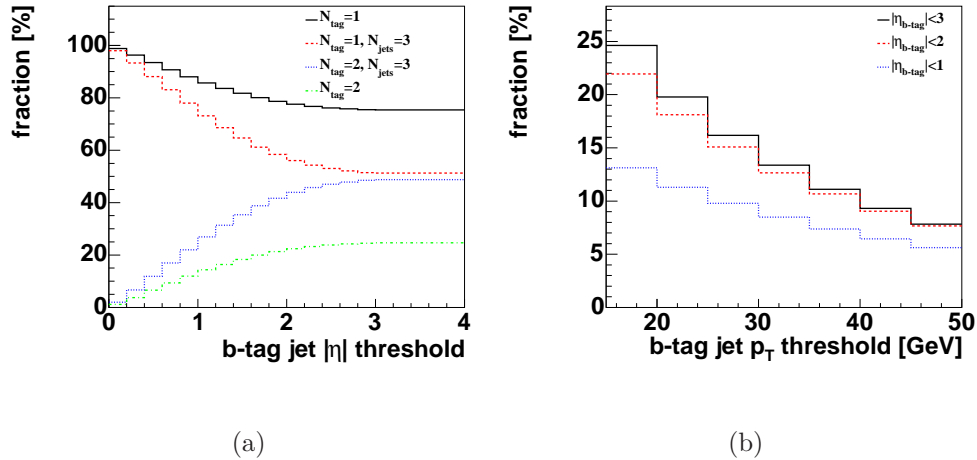


FIG. 23: Fraction of events with one or two  $b$ -tagged jets for the inclusive sample and the exclusive three-jet sample as a function of the pseudo-rapidity cut on the  $b$ -tagged jets (a), and fraction of events with two tagged jets as a function of the  $p_T$  threshold on the  $b$ -tagged jets for three different pseudo-rapidity cuts (b), after the loose selection cuts.

dependence of the total cross section on the jet pseudo-rapidity cut is different between the Born-level and NLO, mostly as a result of the third jet. Figure 6 also shows that not only the cross section but also the jet multiplicity depends strongly on the jet pseudo-rapidity cut. Only for jet pseudo-rapidity cuts above 3 are cross section and jet multiplicities stable.

The fraction of  $b$ -tagged jets also depends strongly on the jet  $p_T$  cut, as shown in Fig. 12. There is a large fraction of events in which the third jet comes from the  $\bar{b}$  quark, especially for low  $b$ -tag  $p_T$  thresholds. This can also be seen in Fig. 23, which shows the dependence of the fraction of events with 1  $b$ -tag and 2  $b$ -tags as a function of the cut on the  $b$ -tagged jet  $p_T$  and  $\eta$ . As before, the fraction of events with 2  $b$ -tagged jets is stable only for pseudo-rapidity thresholds above 3. At that point, about one quarter of the inclusive events contain two  $b$ -tagged jets, and half of the exclusive three-jet events contain two  $b$ -tagged jets. In the following analysis, we shall require at least one  $b$ -tagged jet in the event and do not distinguish the identity of the third jet, unless specified otherwise.

### 1. Kinematic Distribution of the Extra Jet

Initial- and final-state emission of additional gluons occurs before the top quark goes on shell and can thus be considered as “production-stage emission”, while decay-stage emission occurs only after the top quark goes on shell. In principle, an event with an extra jet can thus be classified as production-stage or decay-stage by looking at the invariant mass of the decay products. In production-stage emission events, the  $W$  boson and  $b$  quark momenta will combine to give the top quark momentum. In decay-stage emission events, the gluon momentum must also be included to reconstruct the top quark momentum. This interpretation is exact at the NLO parton level in the narrow width approximation. Finite top width effects can blur the above classification due to interference between production- and decay-stage emission. This classification is nevertheless still useful in our case because the top width of 1.5 GeV is small compared to the hard gluon  $E_T$  cut imposed in the MC calculations. It should be kept in mind that in an actual experiment, the production-decay distinction is further blurred by the experimental jet energy resolution and ambiguities associated with properly assigning partons to jets.

Figure 24 shows the transverse momentum distribution as well as the pseudo-rapidity distribution of the third jet in three-jet events. This jet corresponds to the gluon in about 70% of the events after the loose set of cuts. The transverse momentum distribution of the third jet for those events where that jet corresponds to the  $\bar{b}$  quark (from  $W$ -gluon fusion subprocess) can be seen in Fig. 12. It comprises about 80% of the HEAVY correction after imposing the loose selection cuts, which dominates over LIGHT and TDEC radiative corrections.

As expected, the  $E_T$  distribution is steeply falling for all contributions, but it extends to much higher  $p_T$  values for HEAVY emission. The smaller values of  $E_T$  to which TDEC emission is constrained are again a consequence of the available phase space from the top quark decay. Recall that the top quarks are produced with relatively modest transverse momentum (cf. Fig. 16), so that gluons from the decay do not receive much of a boost. Note also that an increase in the  $p_T$  cut on the jet would result in a further reduction in relative size of the decay contribution compared to production. Figure 24 also shows the distribution in pseudo-rapidity of the extra jet. The third jet radiated from the LIGHT and HEAVY quark lines has a relative larger magnitude in its (non-symmetric) rapidity,

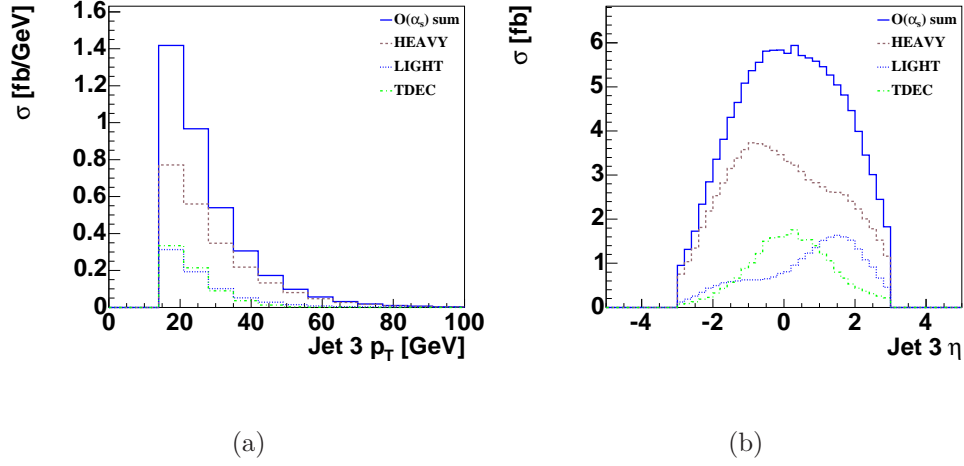


FIG. 24: Transverse momentum (a) and pseudo-rapidity (b) of the third jet after selection cuts for the various  $O(\alpha_s)$  contributions.

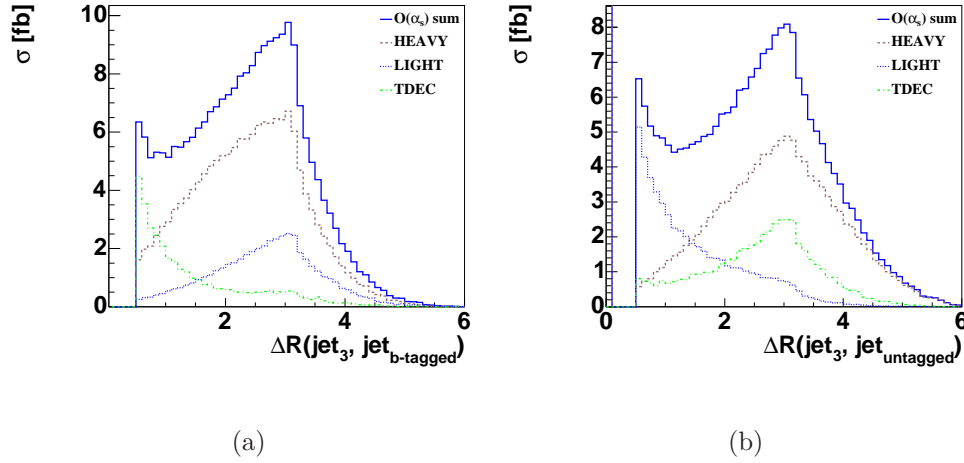


FIG. 25: Separation between the third jet and the tagged jet (a) and between the third jet and the untagged jet (b) after selection cuts for the various  $O(\alpha_s)$  corrections.

as compared to the more central TDEC emission. This is consistent with our intuition that decay-stage radiation, dominated by the gluon radiated from the bottom quark which tends to appear in the central pseudo-rapidity region, is also likely to be produced centrally. However, this TDEC contribution is small and the HEAVY radiation dominates even in the central region.

This tendency of decay-stage radiation to be associated with the final-state  $b$  quark might

lead one to expect that if the extra jet is “near” the  $b$  jet it should be included in the top quark reconstruction, and if it is not then it should be excluded. Figure 25, which shows the angular separation  $\Delta R$  between the extra jet and the leading  $b$ -tagged-jet as well as the leading untagged jet, confirms that the decay-stage radiation peaks close to the leading  $b$ -tagged jet, and production-stage radiation peaks farther away. Figure 25(a) clearly shows that the decay contribution dominates in the low  $\Delta R$  region. This is different from the  $s$ -channel single top process, in which the production contribution dominates over decay emission even in the small  $\Delta R$  region, cf. Fig. 17 of Ref. [18]. A higher  $p_T$  cut on the jet would make this situation worse because it would increase the relative size of the production emission.

Nevertheless, the figure suggests that it might be possible to further improve the top quark reconstruction for exclusive three-jet events. In this paper, we have been using the leading  $b$ -tagged jet to identify the  $b$  quark from the top quark decay, and constraints on  $m_t$  and  $M_W$  to obtain the correct  $p_z^\nu$ . With this procedure the final state can be reconstructed accurately about 84 % of the time in inclusive two-jet events, cf. Fig. 14. Part of the efficiency loss is due to the gluon radiated in TDEC emission, and Fig. 25 indicates that some of this loss could be reclaimed by including the third jet in the top quark reconstruction if it is close to the  $b$ -tagged jet. The actual cut on  $\Delta R$  would need to be tuned to maximize the top quark reconstruction efficiency. However, tuning a prescription for dealing with the extra jet in  $t$ -channel single top quark events is complicated because the effects of multiple emission, hadronization, and detector resolutions will affect the result. For simplicity, we thus chose not to include the third jet in the top quark reconstruction algorithm used in this paper.

In Fig. 25(b), the equivalent distribution in  $\Delta R$  between the extra jet and the untagged jet is also shown, where the LIGHT quark line radiation peaks close to the untagged jet as expected from gluon radiation in the final state. Obviously, the radiation of the HEAVY quark line is dominated by initial state radiation, therefore, its contribution to  $\Delta R(j_3, j_{\text{untagged}})$  is small in the region of small  $\Delta R$ . The peak at zero in this distribution corresponds to events containing two  $b$ -tagged jets in the the  $W$ -gluon fusion subprocess.

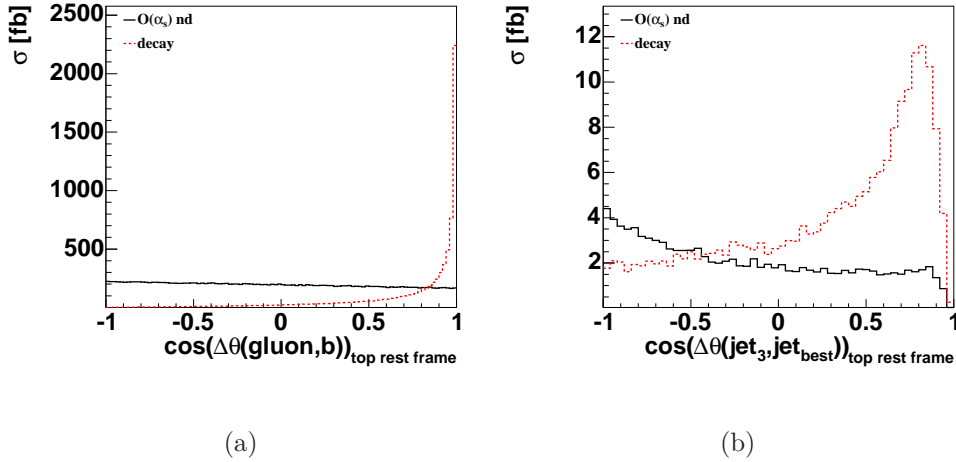


FIG. 26: Angular correlation  $\cos\theta$  between the gluon and the  $b$  quark before any selection cuts using the full parton information (a) and between the third jet and the best jet after selection cuts (b). The solid line shows all  $O(\alpha_s)$  contributions except for the decay part, while the dashed line shows only the  $O(\alpha_s)$  decay contribution.

## 2. Angular Correlation Between the Extra Jet and the Best Jet

As discussed above, the  $\Delta R$  separation between the third jet and the leading  $b$ -tagged jet can be used to distinguish decay-stage emission from production-stage emission. It was shown in Ref. [18] that the best-jet algorithm is effective in reconstructing the  $s$ -channel single top quark event, while retaining the top quark polarization information, but can also distinguish the decay-stage gluon radiation from the production-stage radiation by studying which jets are chosen as the best jets. Similarly, we can also study the correlations between the extra jet and the best jet in  $t$ -channel single top quark events using the best jet algorithm.

Figure 26 (a) shows the angular correlation  $\cos\theta$  between the radiated parton (gluon or  $\bar{b}$ ) and the  $b$  quark at parton level before cuts. Figure 26 (b) shows the same correlation after event reconstruction between the third jet and the best jet. Only events for which the best jet algorithm chooses a two-jet system are included in the figure. In this case there is a clear separation between production-stage and decay-stage emission, and the best jet algorithm can be used to separate the two. This approach thus allows a detailed experimental study of the radiation pattern in top quark decays in the  $t$ -channel single top quark events.



## V. CONCLUSIONS

We have presented a next-to-leading order study of  $t$ -channel single top quark events at the Tevatron, including  $O(\alpha_s)$  QCD corrections to both the production and decay of the top quark. To obtain an accurate prediction of the inclusive rate of  $t$ -channel single top quark production, a modified narrow width approximation has been adopted to link the production of the top quark with its decays (thus preserving top quark spin information) instead of the usual narrow width approximation. The impact of kinematical cuts on the acceptances has been studied for several different sets of cuts. We found that the acceptances are sensitive to the  $\Delta R_{\text{cut}}$  we imposed on the jet cone size and the lepton isolation. With the choice of  $\Delta R_{\text{cut}} = 0.5$ , we found that the difference between the Born-level and NLO acceptances is about 10% for a loose cut set (a) and  $3 \sim 6\%$  for a tight cut set (c). The above difference becomes significantly larger when changing  $\Delta R_{\text{cut}}$  from 0.5 to 1.0.

We categorize the  $O(\alpha_s)$  contributions to the  $t$ -channel single top process into three gauge invariant sets: the light quark line corrections, the heavy quark line corrections and the top quark decay corrections. Keeping track of the different categories facilitates the comparison between event generators and exact NLO predictions.

The  $O(\alpha_s)$  corrections are small in size and contribute about 5.5% of the inclusive cross section at NLO. They do however modify the event kinematics and in particular result in a large fraction of events containing three reconstructed jets in the final state for the loose set of kinematic cuts. The acceptance for  $t$ -channel single top quark events and this fraction of 3-jet events depend strongly on the pseudo-rapidity cut on the jets. Although the radiative corrections to the inclusive  $t$ -channel single top production rate are small, they affect the shape of some of the important kinematic distributions that can be used experimentally to separate the  $t$ -channel single top signal from the various backgrounds, such as the pseudo-rapidity distribution of the spectator jet. We find that the  $O(\alpha_s)$  LIGHT and HEAVY corrections have almost opposite contributions to various pseudo-rapidity distributions, due to the difference in the parton distribution functions between the valence quarks and sea quarks. The former shifts the spectator jet to even higher pseudo-rapidities, while the latter shifts it to more central pseudo-rapidity regions. The summed contributions cause the spectator jet to be even more forward which will change the prediction of the acceptance for  $t$ -channel single top quark events. Also, a large fraction of three jet events contain two

$b$ -jets due to the collinear enhancement in the  $W + g$  fusion process. This implies that higher order corrections need to be calculated in order to correctly predict the behavior of the  $b$ -jet in the small  $p_T$  region.

In order to study top quark properties such as the top quark polarization, induced from the effective  $t$ - $b$ - $W$  couplings, we need to reconstruct the top quark by combining the reconstructed  $W$  boson with the  $b$ -tagged jet. Most of the  $t$ -channel single top quark events contain only one  $b$ -jet in the final state. Thus, we can use the leading  $b$ -tagged jet algorithm to identify the  $b$ -jet in the final state, rather than the best-jet algorithm which is more appropriate for the  $s$ -channel. We found that the leading  $b$ -tagged jet algorithm effectively picks up the correct  $b$ -jet in the event. Since this algorithm makes no assumptions about the other particles in the event, we can use it to also determine the longitudinal momentum of the neutrino ( $p_z^\nu$ ) accurately through a top quark mass constraint. Information about the reconstructed final state can be used to explore correlations between different objects in the event. After reconstruction of the top quark event, we study spin correlations in the top quark decay in three different bases: the helicity basis, the spectator basis, and the beamline basis. We find that the degree of top polarization is very large, especially in the helicity and spectator bases. This is true even after event reconstruction because we are able to reconstruct the top quark final state almost perfectly. As one expects, the degree of top polarization is reduced slightly by the  $O(\alpha_s)$  corrections, both at parton level and after event reconstruction with the loose selection cuts. We also note that using the  $tq$ -frame (the rest frame of the reconstructed top quark and spectator jet) in the helicity basis gives almost the same degree of polarization as in the spectator basis.

Finally, we point out that the above conclusion does not strongly depend on the choice of jet algorithm. We have checked that at the parton level using the Durham  $k_T$  algorithm [33, 34] leads to similar conclusion on the relative importance of the production- and decay-stage gluon emission.

## Acknowledgments

We thank Hong-Yi Zhou for collaboration in the early stage of this project . This work was supported in part by NSF grants PHY-0244919 and PHY-0140106.

## APPENDIX A: TOP QUARK POLARIZATION IN THE S-CHANNEL PROCESS

Above we presented the top quark spin correlations in the helicity basis in the  $t$ -channel using two different definitions for the c.m. frame. In our previous paper on the  $s$ -channel, the degree of top quark polarization in the helicity basis was calculated only in the  $t\bar{b}$  frame (see Sec. IV of Ref. [18]) and given only for inclusive 2-jet events. That frame corresponds to the c.m. frame of the incoming partons strictly speaking only for events without initial or final state gluon radiation. For completeness, we also present here the results for the top quark polarization in the  $s$ -channel single top process for two different c.m. frame definitions. Similar to the  $t$ -channel single top process, we define two reference frames to study the degree of top quark polarization at the parton level in the helicity basis for  $s$ -channel single top quark events.

1.  $t\bar{b}(j)$ -frame: the c.m. frame of the incoming partons. This is the rest frame of all the final state objects (reconstructed top quark and all others jets). In exclusive two-jet events, this frame is the same as that at the Born-level, i.e. reconstructed from summing over momentum of the top quark and non-best-jet. In exclusive three-jet events, this frame is reconstructed by summing over the 4-momenta of top quark, non-best-jet, and the third-jet from the parton level calculation.
2.  $t\bar{b}$ -frame: the c.m. frame of the top quark and non-best-jet. In this case, even in the exclusive three-jet events, the reference frame is constructed by summing over only the 4-momenta of the top quark and non-best-jet. Note that this differs from the  $t\bar{b}(j)$ -frame only in exclusive three-jet events.

We present the resulting top quark polarization in the helicity and optimal bases in Table V for inclusive 2-jet events and in Table VI for exclusive 3-jet events. Similar to the  $t$ -channel, the degree of polarization is larger in the helicity basis in the  $t\bar{b}$  frame. The polarization is reduced when including the possible third jet to reconstruct the c.m. frame in particular for those events where that jet is produced in the initial state, before the virtual  $W$  boson is created. Table VI also shows that the degree of polarization is generally smaller for 3-jet events, which is again similar to the  $t$ -channel.

		$\mathcal{D}$		$\mathcal{F}$		$\mathcal{A}$	
		LO	NLO	LO	NLO	LO	NLO
Helicity basis:	Parton level ( $t\bar{b}(j)$ -frame)	0.63	0.54	0.82	0.77	0.32	0.27
	Parton level ( $t\bar{b}$ -frame)	0.63	0.58	0.82	0.79	0.32	0.29
	Reconstructed events ( $t\bar{b}(j)$ -frame)	0.46	0.37	0.73	0.68	0.21	0.21
	Reconstructed events ( $t\bar{b}$ -frame)	0.46	0.37	0.73	0.68	0.26	0.21
Beamline basis:	Parton level	-0.96	-0.92	0.98	0.96	-0.48	-0.46
	Reconstructed events	-0.48	-0.42	0.74	0.71	-0.24	-0.21

TABLE V: Degree of polarization  $\mathcal{D}$ , polarization fraction  $\mathcal{F}$ , and asymmetry  $\mathcal{A}$  for inclusive two-jet single top quark events, at the parton level and after event reconstruction, in the  $s$ -channel process. Here,  $\mathcal{F}$  corresponds to  $\mathcal{F}_-$  in the helicity basis for left-handed top quarks and to  $\mathcal{F}_+$  in the beamline basis for top quarks with polarization along the direction of anti-proton three momentum, respectively. The  $t\bar{b}g$  frame in the helicity basis denotes the c.m. frame of the incoming partons while  $t\bar{b}$  frame denotes the rest frame of the reconstructed top quark and  $\bar{b}$  quark.

		$\mathcal{D}$	$\mathcal{F}$	$\mathcal{A}$
Helicity basis:	Parton level ( $t\bar{b}g$ frame)	0.45	0.72	0.25
	Parton level ( $t\bar{b}$ frame)	0.49	0.74	0.27
	Reconstructed events ( $t\bar{b}g$ frame)	0.36	0.68	0.21
	Reconstructed events ( $t\bar{b}$ frame)	0.37	0.68	0.21
Beamline basis:	Parton level	-0.81	0.91	-0.45
	Reconstructed events	-0.38	0.69	-0.19

TABLE VI: Degree of polarization  $\mathcal{D}$ , polarization fraction  $\mathcal{F}$ , and asymmetry  $\mathcal{A}$  for exclusive three-jet single top quark events, at parton level and after event reconstruction, in the  $s$ -channel process. Here,  $\mathcal{F}$  corresponds to  $\mathcal{F}_-$  in the helicity basis for left-handed top quarks and to  $\mathcal{F}_+$  in the beamline bases for top quarks with polarization along the direction of anti-proton three momentum, respectively. The  $t\bar{b}g$  frame in the helicity basis denotes the c.m. frame of the incoming partons while the  $t\bar{b}$  frame denotes the rest frame of the reconstructed top quark and  $\bar{b}$  quark.

- 
- [1] A. Stange, W. J. Marciano, and S. Willenbrock, Phys. Rev. **D49**, 1354 (1994), hep-ph/9309294.
- [2] A. Stange, W. J. Marciano, and S. Willenbrock, Phys. Rev. **D50**, 4491 (1994), hep-ph/9404247.
- [3] A. Belyaev, E. Boos, and L. Dudko, Mod. Phys. Lett. **A10**, 25 (1995), hep-ph/9510399.
- [4] Q.-H. Cao, S. Kanemura, and C.-P. Yuan, Phys. Rev. **D69**, 075008 (2004), hep-ph/0311083.
- [5] S. Moretti, Phys. Rev. **D56**, 7427 (1997), hep-ph/9705388.
- [6] K. Odagiri (1999), hep-ph/9901432.
- [7] B. Abbott et al. (DØ), Phys. Rev. **D63**, 031101 (2001), hep-ex/0008024.
- [8] D. Acosta et al. (CDF), Phys. Rev. **D69**, 052003 (2004).
- [9] D. Acosta et al. (CDF), Phys. Rev. **D71**, 012005 (2005).
- [10] T. Tait and C.-P. Yuan, Phys. Rev. **D63**, 014018 (2001), hep-ph/0007298.
- [11] M. C. Smith and S. Willenbrock, Phys. Rev. **D54**, 6696 (1996), hep-ph/9604223.
- [12] G. Bordes and B. van Eijk, Nucl. Phys. **B435**, 23 (1995).
- [13] S. Mrenna and C.-P. Yuan, Phys. Lett. **B416**, 200 (1998), hep-ph/9703224.
- [14] B. W. Harris, E. Laenen, L. Phaf, Z. Sullivan, and S. Weinzierl, Phys. Rev. **D66**, 054024 (2002), hep-ph/0207055.
- [15] Z. Sullivan, Phys. Rev. **D70**, 114012 (2004), hep-ph/0408049.
- [16] J. Campbell, R. K. Ellis, and F. Tramontano, Phys. Rev. **D70**, 094012 (2004), hep-ph/0408158.
- [17] Q.-H. Cao and C. P. Yuan, Phys. Rev. **D71**, 054022 (2005), hep-ph/0408180.
- [18] Q.-H. Cao, R. Schwienhorst, and C. P. Yuan, Phys. Rev. **D71**, 054023 (2005), hep-ph/0409040.
- [19] J. Pumplin et al., JHEP **07**, 012 (2002), hep-ph/0201195.
- [20] Q.-H. Cao and C.-P. Yuan, Phys. Rev. Lett. **93**, 042001 (2004), hep-ph/0401026.
- [21] P. Azzi et al. (CDF Collaborattion) (2004), hep-ex/0404010.
- [22] V. M. Abazov et al. (D0), Nature **429**, 638 (2004), hep-ex/0406031.
- [23] W. T. Giele and E. W. N. Glover, Phys. Rev. **D46**, 1980 (1992).
- [24] W. T. Giele, E. W. N. Glover, and D. A. Kosower, Nucl. Phys. **B403**, 633 (1993), hep-ph/9302225.

- [25] C.-P. Yuan, Phys. Rev. **D41**, 42 (1990).
- [26] J. Alitti et al. (UA2), Phys. Lett. **B257**, 232 (1991).
- [27] G. L. Kane and C.-P. Yuan, Phys. Rev. **D40**, 2231 (1989).
- [28] C.-R. Chen, F. Larios, and C. P. Yuan (2005), hep-ph/0503040.
- [29] G. Mahlon and S. J. Parke, Phys. Rev. **D53**, 4886 (1996), hep-ph/9512264.
- [30] S. J. Parke and Y. Shadmi, Phys. Lett. **B387**, 199 (1996), hep-ph/9606419.
- [31] G. Mahlon and S. J. Parke, Phys. Rev. **D55**, 7249 (1997), hep-ph/9611367.
- [32] G. Mahlon (1998), hep-ph/9811219.
- [33] S. Catani, Y. L. Dokshitzer, and B. R. Webber, Phys. Lett. **B285**, 291 (1992).
- [34] S. D. Ellis and D. E. Soper, Phys. Rev. **D48**, 3160 (1993), hep-ph/9305266.